Multi-phase dolomitization and recrystallization of Middle Triassic shallow marine–peritidal carbonates from the Mecsek Mts. (SW Hungary), as inferred from petrography, carbon, oxygen, strontium and clumped isotope data

Georgina Lukoczki[a*], János Haas[b], Jay M. Gregg[a], Hans G. Machel[c], Sándor Kele[d], Cédric M. John[e]

[a]Boone Pickens School of Geology, Oklahoma State University, 105 Noble Research Center, Stillwater, OK 74078, USA (*Corresponding author e-mail: gina.lukoczki@okstate.edu)

[b]MTA-ELTE Geological, Geophysical and Space Science Research Group, Pázmány Péter sétány 1/c, Budapest, 1117, Hungary

[c]Department of Earth and Atmospheric Sciences, University of Alberta, 1-26 ESB, Edmonton, AB, T6G 2E3, Canada

[d]Research Centre for Astronomy and Earth Sciences, Institute for Geological and Geochemical Research, Hungarian Academy of Sciences, Budaörsi út 45, Budapest, 1112, Hungary

[e]Department of Earth Science and Engineering, Imperial College London, Royal School of Mines, Prince Consort Rd, Kensington, London SW7 2BP, UK

ABSTRACT

Shallow marine to peritidal carbonates of the Triassic Csukma Formation in the Mecsek Mts. of SW Hungary are made up of dolomites, limestones and dolomitic limestones that show evidence of a complex diagenetic history. Integration of petrographic, conventional stable oxygen and carbon isotope, clumped isotope, and strontium isotope data with the paleogeography, paleoclimate, and burial history of the region revealed four major diagenetic stages. Stage 1: The

peritidal carbonates were dolomitized penecontemporaneously during the Middle Triassic by refluxing evaporatively concentrated brines. Stage 2: Increasing burial during the Late Triassic–Jurassic resulted in recrystallization of the Kán Dolomite Member in an intermediate burial setting. Stage 3: During the Early Cretaceous seawater was drawn down and circulated through rift-related faults, causing renewed recrystallization of the Kán Dolomite Member as well as dolomitization of the Kozár Limestone Member and the underlying limestones in a deep burial setting, but only in the vicinity of the faults. Stage 4: During the Late Cretaceous and Cenozoic thrusting resulted in tectonic expulsion of basinal fluids and precipitation of multiple saddle dolomite cement phases near the faults.

The results of this study imply that the clumped isotope method integrated with other geochemical data can successfully be applied to identify the nature and potential sources of extra-formational diagenetic fluids responsible for dolomitization and recrystallization. This study provides conclusive evidence for multi-phase dolomitization and dolomite recrystallization over several millions of years (Middle Triassic through Early Cretaceous) and several thousands of meters of burial in the Csukma Formation in SW Hungary. Furthermore, this study is the first to identify fault-controlled dolomitization by circulating Cretaceous seawater within Triassic carbonates of central Europe, further supporting the viability of the interpretation of dolomitization by seawater initially drawn down and then geothermally circulated through faults in extensional basins.

Key words: dolomitization, recrystallization, paleogeography, burial history, stable isotope, clumped isotope, strontium isotope, Mecsek Mts.

1. Introduction

Dolomite rocks (also known as dolostones) comprise a large portion of the world's hydrocarbon and potable water reservoirs and thus have been the focus of long-term research interest. Dolomitization, which is the process of calcite replacement by dolomite, occurs in a number of geological environments predominantly through the addition of magnesium (Mg^{2+}), introduced by aqueous fluids, to limestone in some form of advection (e.g., Machel, 2004). Most dolomites that formed in near-surface settings are metastable upon formation (commonly referred to as very high magnesium calcites (VHMC) or protodolomites; Machel 2004; Gregg et al. 2015), and transform into more stable dolomite via recrystallization or, albeit rarely, they persist as metastable phases over geological time (e.g., Land, 1980; Mazzullo, 1992; Gregg et al., 2015). During recrystallization the overall mineralogy of the rock does not change; however, a number of chemical, crystallographic and physical properties may be reset (cf. concept of significant vs. insignificant recrystallization; Machel, 1997). Therefore, the chemical and/or physical properties of recrystallized dolomites may no longer reflect the mechanism of dolomitization but represent the geological environment and/or process of recrystallization. Thus, not recognizing recrystallization may cause inaccurate genetic interpretation of dolomitization (Machel, 1997). The nature and extent of recrystallization is controlled by the geological evolution of the area; therefore, precise interpretation of the geological evolution of dolomite geobodies is crucial for reservoir characterization, since recrystallization may significantly alter the porosity and permeability of dolomites (Al-Aasm and Packard 2000; Sun, 1995; Machel, 2004).

Even though numerous case studies demonstrated recrystallization of dolomites of ages ranging from Paleozoic to Holocene, identifying the dolomitizing and recrystallizing fluids and

processes remains challenging. Typically, initial dolomitization of peritidal carbonates is interpreted to have occurred via evaporatively concentrated seawater (e.g., Machel, 2004). In some cases, the initial reflux/sabhka dolomitization was interpreted to have been followed by recrystallization in meteoric or mixed meteoric–marine fluids (e.g., Spötl and Burns, 1991; Kupecz and Land, 1994). A second recrystallization event by warm/hot extra-formational fluids is often invoked to explain the current petrographic and/or geochemical signatures (e.g., Spötl and Burns, 1991; Montanez and Read, 1992; Kupecz and Land, 1994; Nader et al., 2004). Even though the dolomitizing capability of mixed meteoric–marine fluids has long been questioned (e.g., Hardie, 1987; Machel, 2004), a few authors have argued that initial partial dolomitization may occur with the aid of such fluids, and complete dolomitization of the investigated rock sequences was later achieved via interaction with warm basinal fluids that also recrystallized the pre-existing dolomites (e.g., Banner et al., 1988; Durocher and Al-Aasm, 1997). Basin-wide burial dolomitization of some Devonian carbonates of Western Canada was locally followed by recrystallization in hydrothermal fluids, also referred to as 'hydrothermal alteration' (e.g., Lonnee and Machel, 2006), related to tectonic expulsion (e.g., Machel et al., 1996) and/or to topographically driven flow (Qing and Mountjoy, 1994). On the other hand, recrystallization has also been identified to occur extremely early and under near-surface conditions. An example is a study of Holocene samples from Belize, which revealed that surface energy-driven recrystallization may occur within a few thousand years in the topmost meter of the sediment (Gregg et al., 1992).

Carbonate clumped isotope (Δ_{47}) thermometry (e.g., Ghosh et al., 2006; Eiler, 2007) is a novel method to investigate the nature and origin of diagenetic fluids. The calibration and limitations of the dolomite clumped isotope thermometer for diagenetic temperatures is now sufficiently well-established (see Bonifacie et al., 2017, and references therein). Comparing temperatures obtained from fluid inclusions and clumped isotopes supports the reliability of the dolomite clumped isotope

thermometer (e.g., Millán et al., 2016; Came et al., 2017, Honlet et al., 2018), and over the past decade, an increasing number of studies have demonstrated the usefulness of this method in investigating dolomite diagenesis. A major advantage of this method is to be able to determine the temperature and oxygen isotope composition of the diagenetic fluids where fluid inclusion measurements are not feasible. Such is the case with very fine to fine crystalline dolomites (i.e., dolomicrites), low-temperature cements with single phase fluid inclusions, or where fluid inclusions are not present or their size is too small to observe phase changes. Successful applications of the clumped isotope thermometer include to determine the nature and origin of the dolomitizing (e.g., Ferry et al., 2011), or recrystallizing fluids (e.g., Sena et al., 2014; Loyd et al., 2015), and to reconstruct thermal and fluid flow histories (e.g., MacDonald et al., 2018; Mangenot et al., 2018). The method can provide especially useful insights when applied in combination with other methods (e.g., with U-Pb dating, Lawson et al., 2018).

Shallow marine–peritidal carbonates of the Csukma Formation in the Mecsek Mts. of SW Hungary (Figs. 1, 2) are made up of varied dolomites, limestones and dolomitic limestones, and show evidence of a complex diagenetic history. The peritidal inner ramp succession is completely dolomitized, whereas the extent of dolomitization of the middle ramp shoal deposits varies from none to complete. Even though the Csukma Formation has been characterized in basic sedimentological and stratigraphic studies (e.g., Török, 1998a; Haas et al., 2002), detailed information about their diagenetic evolution, and in particular, their dolomitization history, is lacking.

Very little is known about the Triassic dolomites of southern Hungary (structurally Tisza Mega-Unit, Fig. 1a) in general, in striking contrast to the extensively studied Triassic dolomites in northern Hungary (structurally Alcapa Mega-Unit, Fig. 1a) (see review of the dolomitization processes in Haas et al., 2017). In northern Hungary, the Triassic succession is of Alpine character,

i.e., similar to the Triassic formations of the Alps, which were deposited in the northwestern part of the Tethys ocean (Feist-Burkhardt et al., 2008; Haas et al., 2017). In southern Hungary, however, the Triassic succession is similar to the epicontinental deposits of the Germanic Basin (Török, 2000a). In the southwestern part of this region, Török (2000b) studied the origin of dolomitic mottles and of saddle dolomite cements in the Middle Triassic Zuhánya Limestone Formation (Fig. 2) in the Villány Hills (Tisza Mega-Unit, Villány-Bihor Unit) (VH in Fig. 1a). Dolomite in the mottles was interpreted to have been formed from marine-derived pore waters during burial in a partly closed diagenetic system fairly soon after deposition and at relatively shallow depths, whereas the saddle dolomite cements likely precipitated during maximum burial of the succession in the Cretaceous (Török, 2000b). Another study of note is by Garaguly et al. (2018), who investigated the dolomitization of the Middle Triassic Szeged Dolomite Formation (time-equivalent to the Csukma Formation) within the Békés-Codru Unit of the Tisza Mega-Unit in southeast Hungary (Fig. 1a). These authors found that the Szeged Dolomite was formed as a result of early reflux dolomitization, later altered by hydrothermal recrystallization.

The present paper provides a detailed interpretation of the various dolomitization and recrystallization processes that affected the Middle Triassic Csukma Formation on the basis of detailed petrographic and geochemical investigation. In addition, our study demonstrates that integration of clumped isotope data with other geochemical information can help discriminate various diagenetic fluids and processes that are otherwise difficult to distinguish, such as meteoric alteration versus burial dolomitization/recrystallization, two processes that can lead to similar petrographic features and isotopic composition of the resulting dolomite.

2. Materials and methods

A total of 160 thin sections were prepared from samples collected from seven locations in the Mecsek Mts. (two boreholes and five outcrops). The sampling locations are shown in Figure 1b and listed in Table 1. The thin sections were investigated in normal transmitted light on an Olympus-BX51 microscope for their petrographic features. The crystal size categories were assigned based on the scale published by Folk (1959). Dolomite textures were classified using the system of Sibley and Gregg (1987) as modified by Wright (2001) (see Machel, 2004). Selected thin sections were stained in a solution of Alizarin red-S and potassium ferricyanide to distinguish calcite, Fe-calcite, dolomite, Fe-dolomite/ankerite, using the method of Dickson (1966).

Cathodoluminescence (CL) microscopy was performed on 83 polished thin sections using a MAAS-Nuclide ELM-3 cold-cathode luminoscope at the Department of Physical and Applied Geology, Eötvös Loránd University, and using a CITL MK5-1 cold-cathode optical cathodoluminescence system at the Boone Pickens School of Geology, Oklahoma State University, with operating conditions of 8–12 keV and 0.5–0.7 mA. The samples for CL study were selected based on their dolomite texture types and cement contents.

Stable isotope measurements ($\delta^{18}O$, $\delta^{13}C$) were performed on 101 micro-drilled calcite and dolomite powder samples (five calcite cement, 17 limestone, 14 saddle dolomite, 65 matrix dolomite samples, which represent the various dolomite types and cement phases). Analyses were performed at three laboratories. At the Institute for Geological and Geochemical Research, Hungarian Academy of Sciences and at Oklahoma State University the measurements were performed on a Finnigan Delta Plus XP Isotope ratio mass-spectrometer (IRMS), and a setup of a Thermo Delta Plus IRMS coupled to a Gas Bench II was used by Pegasus Technical Services Inc.

(Cincinnati, OH, USA). All laboratories used both international (NBS-18, NBS-19) and internal laboratory standards. Reproducibility in all laboratories was better than ±0.1‰; however, differences measured on replicates of the same samples in the various laboratories were not consistent and therefore did not allow for correction of values across the various laboratories. Nevertheless, the data can be interpreted in a meaningful way because the differences between the various phases exceed the differences found by inter-lab comparison of the data. Mean values of the measurements are reported relative to the Vienna Pee Dee Belemnite standard (V-PDB ‰).

Strontium isotope composition ($^{87}Sr/^{86}Sr$) was analyzed on 10 dolomite samples (eight replacive dolomite samples, two saddle dolomite cement samples), and on two limestone samples, at the University of Kansas Radiogenic Isotope Laboratory using a VG Sector thermal ionization mass spectrometer with ±0.000014 error at a 95% confidence interval, and at the Canadian Centre for Isotopic Microanalysis at the University of Alberta using a VG 354 thermal ionization mass spectrometer with analytical precision better than 0.000024 (2σ). Systematic differences in the results across these two laboratories were corrected.

In this study, the temperatures of crystallization were determined only via the clumped isotope method. Fluid inclusion paleothermometry was not feasible due to crystal size limitations in the very fine to fine crystalline dolomites, and due to the small size of the two-phase inclusions in the medium to very coarse crystalline phases.

Carbonate clumped isotopes were measured on seven matrix dolomite samples in the Qatar Stable Isotope Laboratory at Imperial College London on a Thermo Fisher MAT 253 isotope ratio mass spectrometer in dual inlet mode, using the methodology described in Dale et al. (2014). For the evaluation of geological processes, the Δ_{47} values were converted to temperature using the calibration of Davies and John (2018) and are presented in °C. The $\delta^{18}O$ values of the parent fluids

were calculated using the calibration of Horita (2014) and the results are reported relative to the Vienna Standard Mean Ocean Water standard (V-SMOW ‰).

3. Geological setting

3.1. Sedimentology and stratigraphy

The study area is located within the Pannonian Basin, in southwestern Hungary, comprising a part of the Tisza Mega-Unit (herein referred to as Tisza MU) (Bleahu et al., 1994) (Fig. 1a). During the Middle Triassic, the investigated area was located on the northwestern shelf of the Neo-Tethys, around the 30° N latitude, and it was dominated by subtropical trade winds (Török, 2000a; Szulc, 2000; Götz et al., 2003; Feist-Burkhardt et al., 2008). This paleogeographic setting resulted in semiarid to semihumid climates during Late Anisian–Early Ladinian times (Török, 1998a; Viczián, 1995; Haas et al., 2012), and in a sedimentation pattern similar to that in the Germanic Basin (Török, 2000a; Götz and Török, 2008).

The Variscan (late Paleozoic) crystalline basement in the Tisza MU is covered by molasse-type sequences of late Carboniferous to Permian age (Haas and Péró, 2004). During the Early Triassic fluvial and deltaic siliciclastic sedimentation prevailed, which was followed by the formation of carbonate ramp deposits during the Middle Triassic, suggesting a relative sea level rise (Török, 1998a). A relative sea level fall near the end of the Middle Triassic led to the deposition of the shallowing upward succession of the Csukma Formation (Konrád, 1998) (Fig. 2). Fluvial-deltaic sedimentation returned during the Late Triassic, and a more than 1,000 m thick coal-bearing sequence was formed during the Early Jurassic in fluvial, lacustrine and palustrine environments (Némedi Varga, 1998). The coal-bearing sequence is overlain by upper Lower to lower Middle Jurassic pelagic marls, and the early Middle and Late Jurassic is characterized by

siliceous and carbonate sedimentation in deep marine setting (Némedi Varga, 1998). During the Early Cretaceous, continental rift-related basaltic igneous activity characterized the studied region (Harangi et al., 1996). These igneous rocks are locally overlain by Lower Cretaceous coarse-grained clastics rocks that derived from the volcanic buildups, as well as carbonate and fine-grained siliciclastic rocks representing shallow to deep marine depositional environments, respectively (Császár, 1998). Paleogene deposits are generally missing in the area except for localized occurrences of continental clastic sediments (Wéber, 1982), and Neogene sediments are also only preserved locally: the lower Miocene sediments are of alluvial fan and fluvial origin, the middle Miocene sediments are open marine limestones and shales, and the upper Miocene–Pliocene is characterized by lake-delta deposits (Magyar et al., 1999).

3.2. Geodynamic evolution

The Triassic succession of the Mecsek Mts. was deposited on the northern passive margin of the Neo-Tethys (Haas and Péró, 2004). The opening of the Neo-Tethys in the Middle Triassic was accompanied by complex block movements in the region of the Mecsek Mts. (Konrád, 1998). Unlike in the Southern Alps, the Middle Triassic tectonic activity in the Mecsek Mts. did not result in volcanism (cf., Bellieni et al., 2010; Lukoczki et al., 2015). In connection with the Alpine Tethys rifting, detachment of the Tisza MU from the European platform started in the Late Triassic (Haas and Péró, 2004). Related synsedimentary tectonic movements resulted in the development of a half-graben structure in the area of the Mecsek Mts., which in turn resulted in significant differences in the thickness of the sedimentary successions deposited in different parts of this basin during the Late Triassic and Jurassic (Némedi Varga, 1983). During the Early Cretaceous, the rifting was accompanied by submarine mafic igneous activity (e.g., Harangi et al., 1996; Haas and Péró, 2004). Igneous rocks (alkali basalt, trachybasalt, tephrite and phonolite) from this activity

occur extensively in the Eastern Mecsek Mts., whereas in the Western Mecsek Mts. they occur only subordinately (Budai et al., 2014). These igneous rocks can be found in a belt ca. 250 km long and 50 km wide, striking SW–NE within the Tisza MU (Bilik, 1980). The igneous intrusions caused widespread hydrothermal alteration in the host rocks (Jáger, 2015).

Tectonic extension changed to compression/transpression around the middle of the Cretaceous period, and it resulted in stacking of north-vergent nappes (thrust sheets) (Bleahu et al., 1994). This Late Cretaceous tectonic phase formed the most prominent structural pattern of the Mecsek Mts. as found today: the Western Mecsek forms an anticline, whereas the Eastern Mecsek is a syncline.

The Pannonian Basin came into being as a result of a very complex tectonic evolution during the Cenozoic. Csontos et al. (2002) identified five tectonic phases: (i) thrusting and transpression during the latest Paleogene and earliest Miocene, which created the Northern Imbricates wrench zone in the northern part of the Mecsek Mts. (Fig. 1b); (ii) strike-slip faulting and subsidence during the middle Miocene; (iii) around the end of the middle Miocene (end of the Sarmatan/Serravallian) thrusting and folding occurred near the Northern Imbricates and the Hetvehely zone (Fig. 1b); (iv) transtension during the early Pannonian (Tortonian); and (v) a major inversion created transpressive wedges and resulted in a still ongoing folding and uplift of the Mecsek Mts.

4. Results

4.1. Petrography

4.1.1. Very fine to fine crystalline dolomites

Very fine to fine crystalline dolomites (7 to 65 μm) of the Kán Dolomite Member (Fig. 2) occur at locations GF-1, RV, HR and VP-2 (Fig. 1b). These dolomites are thin bedded or laminated (Fig. 3a), and locally contain mm to cm size rip-up clasts. Teepee structures (10 to 20 cm high) can be recognized in outcrop (Fig. 3b). In exceptional cases, some thin bedded to laminated dolomudstones contain needle-shaped quartz pseudomorphs likely after gypsum (Fig. 3c). The massive dolomudstones typically contain round or elongate moldic pores (range in size from ca. 100 μm up to a few mm) (Fig. 3d), which are either open or are lined or filled with fine crystalline (25 to 50 μm) planar, zoned dolomite cement within a homogenously dull red dolomite matrix (Fig. 3e–f). The final pore-occluding phase in the larger moldic pores generally is blocky calcite (up to a few mm).

4.1.2. Medium to very coarse crystalline dolomites

Medium to very coarse crystalline (76 to 395 μm), unimodal to polymodal, planar-s to nonplanar-a dolomites occur at all studied locations. The very fine to fine crystalline dolomudstones (see Section 4.1.1.) alternate with medium crystalline (76 to 133 μm), planar-s dolomites with poorly preserved ooid-peloidal grainstone/packstone fabrics (Fig. 4a). These tight, medium crystalline, planar-s dolomites are typically comprised of inclusion-rich dolomites with uniformly mottled CL patterns or of dolomites with cloudy cores and clear rims. The cloudy cores have mottled CL appearance, whereas the limpid rims are either zoned or homogeneously dull red (Fig. 4b–c).

The coarse to very coarse crystalline (186 to 395 μm) dolomites occur in irregular bodies near fractured zones within the fine crystalline dolomites at location HR (5 to 10 m thick/wide) and location AT (tens of m), as well as in drill cores of location VP-2 (tens of cm to few m). Poor outcrop conditions make exact determination of the spatial distribution of the coarse to very coarse crystalline dolomite bodies difficult. Similarly, the poor outcrop conditions make it impossible to

provide statistically reliable measurements of the fracture orientations. These dolomites are largely fabric-destructive and are either tight or porous. Generally, the tighter dolomites are planar-s to nonplanar-a. The more porous dolomites typically have planar-s textures with intercrystal pores (Fig. 4d). The CL pattern of the coarse crystalline matrix dolomites is variable: they either display homogenous CL (from very dull to bright) or they display a mottled or blotchy appearance. The transition between the various types is sharp or gradual. At location HR (Fig. 1b), small irregular bodies (1 to 2 m thick/wide) of friable dolomite can be found within the massive coarse crystalline dolomite (Fig. 4e). This friable dolomite easily disintegrates between fingers to small crystal clusters, individual crystals or crystal fragments (Fig. 4f).

At location VA (Fig. 1b), a crinoid floatstone fabric is preserved in fine to coarse crystalline dolomites, as recognized by the presence of biomolds and partially preserved crinoid fragments (Fig. 4g), which are either mimetically replaced or are replaced by fine to coarse crystalline dolomite with blotchy CL. The matrix of these dolofloatstones is composed of planar-s dolomite. Parts of the matrix appear coarse crystalline and nearly limpid with a CL pattern of blotchy core overgrown by homogeneous rim, whereas the finer crystalline, more inclusion-rich crystals display homogeneous dull CL (Fig. 4h–i).

4.1.3. Limestones and dolomitic limestones

The Kozár Limestone Member, which is coeval with the lower part of the Kán Dolomite Member (Fig. 2), is made up of alternating beds of mudstone, bioclastic-peloidal-ooid grainstone, packstone, and wackestone microfacies. The uppermost part of the Zuhánya Limestone Formation, which underlies both the Kán Dolomite Member and the Kozár Limestone Member (Fig. 2), is made up of similar microfacies and is discernible from the Kozár Limestone Member primarily based on their stratigraphic position and their differing bioclast assemblages. Both limestones are

locally partially to completely replaced by dolomite, and the dolomites show similar petrographic features within the two limestones. Dolomite occurs associated with all of the observed limestone microfacies. The Kozár Limestone is partially dolomitized at locations MR and AT (Fig. 1b), and the Zuhánya Limestone is partially dolomitized at location HR (Fig. 1b), where fine to coarse crystalline (20–190 μm) planar-p dolomite crystals are randomly distributed, or they occur along microfractures replacing the limestones (Fig. 5a–b). Some of the dolomite crystals are present as calcite pseudomorphs after dolomite ('dedolomite') (Fig. 5c). In the Zuhánya Limestone, the allochems are always non-mimetically replaced by dolomite (Fig. 5d). At locations AT and HR, where dolomitization is locally more extensive, the dolomites also occur in large (meters to tens of meters), irregular bodies within the limestones. The petrographic features of these dolomites are similar to those occurring in irregular bodies within the fine crystalline dolomites (see Section 4.1.2.).

4.1.4. Saddle dolomite cements

An overall small volume of open space filling saddle dolomite occurs in the fine crystalline dolomites, commonly as cement in veins that cross-cut the fine crystalline matrix dolomites. Larger volumes of saddle dolomite cements are associated with the coarse crystalline replacive dolomites. Based on their CL, multiple generations of saddle dolomites are discernible at each location. Complex and unique CL zonation patterns (homogenous, mottled, simple concentric and oscillatory concentric zonation with various CL intensities) (Fig. 6a–h) make correlation of the various saddle dolomite phases difficult even within the same location. Some zones within saddle dolomite cements are selectively replaced by calcite (Fig. 6i).

4.1.5. Calcite cements

Various calcite cement phases can be distinguished within the dolomite rocks, based on their petrographic appearance. White to colorless, coarse crystalline (up to few mm), 'massive' or blocky calcite (CAL-1 and CAL-2) with dull to bright orange, blotchy CL occludes voids, fills fractures, and forms cement in breccias (Fig. 7a–b). Occasionally, this generation of calcite forms large (up to 2 cm) euhedral scalenohedra (Fig. 7c). Transparent, colorless, coarse crystalline (typically up to ca. 500 μm), blocky calcite fills fractures (Fig. 7d) and it also is present as a final pore-occluding phase in some vugs. This calcite has typically dull or non-luminescent CL (Fig. 7e). Brownish, coarse crystalline (up to few mm), blocky (Fig. 7f–g) or bladed (Fig. 7h) calcite (CAL-3) fills fractures and lines vugs. This calcite is either non-luminescent or displays bright yellow/non-luminescent simple or oscillatory concentric CL zonation (Fig. 7g). Non-luminescent calcite also occurs in stylolites (Fig. 7i).

4.2. Isotope geochemistry

4.2.1. Carbon and oxygen isotopes

The carbon and oxygen isotope data are plotted in Figure 8 and tabulated in Table 2. Matrix dolomite $\delta^{18}O_{dol}$ values fall in a wide range from –12.6‰ to –2.0‰, whereas their $\delta^{13}C$ values fall within a narrower range from 0.1‰ to 4.2‰. Generally, the fine(r) crystalline dolomites have higher $\delta^{18}O_{dol}$ values whereas the coarse(r) crystalline dolomites have lower $\delta^{18}O_{dol}$ values (Fig. 8). The isotope values of saddle dolomite cements overlap with those of the medium to coarse crystalline matrix dolomites (Fig. 8), the former having $\delta^{18}O_{dol}$ values that range from –15.4‰ to –6.2‰ and $\delta^{13}C$ values that range from –1.0‰ to 3.7‰. The calcite cement $\delta^{18}O_{cal}$ values fall

within the interval from –20.5‰ to –6.2‰, and the $\delta^{13}C$ values are within –8.5‰ and –0.3‰. The $\delta^{18}O_{cal}$ values of the limestone matrix range from –9.9‰ to –7.2‰, whereas their corresponding $\delta^{13}C$ values range from –3.3‰ to 2.2‰.

4.2.2. Clumped isotopes

Temperatures and $\delta^{18}O_{fluid}$ were determined from carbonate clumped isotope (Δ_{47}) data (Table 2). The Δ_{47} values range from 0.478 to 0.611‰, corresponding to calculated temperatures that range from 50 to 130 °C. Based on the obtained temperatures, two distinct dolomite groups can be distinguished (Fig. 9). The fine crystalline dolomites fall within the range of 50 to 67 °C, whereas the medium to coarse crystalline, planar-s to nonplanar-a dolomites range from 107 to 130 °C. The $\delta^{18}O_{fluid}$ values of the precipitating fluids calculated from the clumped isotope results range from 1.3‰$_{V\text{-}SMOW}$ to 4.3‰$_{V\text{-}SMOW}$. The values of the fine and the medium to coarse crystalline dolomites overlap, but the values of the very fine and fine crystalline dolomites are somewhat higher (2.0 to 3.0‰$_{V\text{-}SMOW}$) than the medium to coarse crystalline dolomites (1.3 to 2.6‰$_{V\text{-}SMOW}$), with the exception of an outlier coarse crystalline dolomite from location VA, which has the highest value (4.3‰$_{V\text{-}SMOW}$) (Fig. 9, Table 2).

4.2.3. Strontium isotopes

The $^{87}Sr/^{86}Sr$ values of all samples fall within a rather narrow range from 0.70780 to 0.70823 (Figs. 10, 11, Table 2). Typically, the lower values represent the medium to coarse crystalline dolomites (0.70797 to 0.70780), while the higher values represent the very fine to fine crystalline dolomites (0.70813 to 0.70819) (Fig. 11). The values of the two limestone matrix samples fall near the middle of the range of the dolomite samples, separating the very fine to fine and the medium to coarse

crystalline dolomite values (Fig. 11). However, one saddle dolomite cement from location VA has the highest value observed (Table 2). The matrix dolomite from the same sample with the saddle dolomite cement from this location has the lowest value within the data set (Table 2). Therefore, both the lowest and the highest Sr isotope values were measured from different parts of the same sample (matrix dolomite and saddle dolomite cement, respectively).

5. Discussion

Petrographic and geochemical characteristics of the studied sedimentary succession suggest multiple phases of dolomitization, dolomite recrystallization, and cementation processes. The major diagenetic events are summarized in Fig. 12 and are discussed in detail in the following sections. Differentiation of diagenetic environments into near-surface, intermediate, and deep follows the classification of Machel (1999).

5.1. Near-surface dolomitization

Sedimentological features of the Kán Dolomite Member such as teepee structures, rip-up clasts, pseudomorphs after gypsum, and laminated dolomudstones (Fig. 3), suggest that this unit was deposited in a peritidal environment, in accordance with earlier sedimentological studies (e.g., Török, 1998a). The molds and pseudomorphs after gypsum suggest that the salinity of the pore water reached gypsum saturation at least periodically. The fluid compositions calculated from the clumped isotope data of the very fine and fine crystalline dolomites (2.0 to 3.0‰$_{V\text{-}SMOW}$) (Fig. 11) correspond closely to values measured in evaporatively concentrated brines from supratidal settings, even though the values represent only the lower end of the range characterizing such fluids (ca. +1‰$_{V\text{-}SMOW}$ to +10‰$_{V\text{-}SMOW}$, typically around +2‰$_{V\text{-}SMOW}$ to +5‰$_{V\text{-}SMOW}$) (e.g., Gat

and Levy, 1978; McKenzie, 1981; Major et al., 1992, Machel and Buschkuehle, 2008). Possible explanations of the oxygen isotopic composition calculated for the Kán Dolomite include a less arid climate (cf. Major et al., 1992), and meteoric influx that would have lowered the $\delta^{18}O$ of the seawater, as suggested by Korte et al. (2005) to explain the lower $\delta^{18}O$ values of Middle Triassic carbonates of the Germanic Basin. A minor meteoric input may also be reflected in the Sr isotope values of the very fine to fine crystalline dolomites ($^{87}Sr/^{86}Sr$=0.70813 to 0.70819) (Fig. 11), which are slightly elevated with respect to normal marine values of the Middle Triassic Neo-Tethys Ocean (ca. 0.70772 around the Anisian/Ladinian boundary) (Korte et al., 2003) (Fig. 10). Elevated Sr isotope values characterize also the regionally extensive Upper Muschelkalk carbonates (Middle Triassic in the Germanic Basin) (Korte et al., 2003; Adams et al., 2018), which are coeval with the Csukma Formation. Elevated Sr isotope values could have been derived from meteoric influx from exposed Variscan crystalline rocks in the hinterland through riverine discharge into the epicontinental sea of the Germanic Basin (Korte et al., 2003). However, in the Csukma Formation such meteoric influx appears to have been relatively moderate, probably due to the connection of the sedimentary environment to the Neo-Tethys Ocean. Therefore, the estimated fluid composition is in agreement with paleogeographic and paleoclimatic reconstructions (e.g., Szulc, 2000), which claim that the region of the Mecsek Mts. was situated in a transitional position between the Germanic Basin ('Muschelkalk Sea') and the Neo-Tethys at around the 30° paleolatitude, and that semiarid to semihumid climates prevailed during Middle Triassic times.

The two most likely dolomitization models to explain dolomitization of the Kán Dolomite Member are the sabkha and the reflux models, whereby processes of both models may have been involved, albeit to differing degrees.

Sabkha dolomitization generally produces very limited amounts of dolomite in thin beds (e.g., Machel 2004). Therefore, it is highly unlikely that sabkha processes led to complete

dolomitization of the Kán Dolomite Member (up to ca. 300 m thickness). However, sabkha dolomitization may have contributed to the early dolomitization of the Kán Dolomite Member by virtue of producing very small amounts of disseminated (proto)dolomite that served as nuclei for subsequent, more extensive dolomitization (cf., Gregg et al., 2015; Kaczmarek et al., 2018).

The bulk of the dolomite of the Kán Dolomite Member likely was produced by reflux dolomitization, a mechanism originally proposed by Adams and Rhodes (1960) and later verified by virtue of case studies and reaction transport modeling as a viable mechanism to generate large volumes of regionally extensive dolomites (e.g., Montanez and Read, 1992; Jones et al., 2003; Machel, 2004). The limited evidence of evaporation (small amounts of gypsum pseudomorphs) suggests that the salinity of the pore water was typically mesohaline (salinity between normal seawater and gypsum saturation) and occasionally hypersaline up to at least gypsum saturation. Brine generation is assumed to have been continuous during the latest Anisian–Ladinian, whereby minor changes in relative sea level led to shifts in the area of brine generation. Dolomitization was penecontemporaneous with deposition and likely restricted to the upper 2 to 3 m of the succession (cf. modelling results of Jones et al., (2003) on the Devonian Grosmont Formation for analogy). In this manner, dolomitization proceeded bed-by-bed during the estimated relatively long duration of the reflux circulation (latest Anisian through most of the Ladinian), with overall rather low depositional rates (estimated ca. 10 cm/ky based on the thickness and age of the succession).

In contrast, the middle ramp carbonates of the Kozár Limestone Member contain only dolomites with characteristic high temperature textures (fabric destructive, medium to coarse crystalline, planar-s to nonplanar-a dolomites associated with various microfacies) (Fig. 5). The apparent lack of early dolomitization of these middle ramp carbonates can be explained by the interaction of geothermal and reflux circulation similar to the situation modelled by Jones et al. (2004), which showed that reflux circulation is restricted to the inner ramp, whereas the more distal

parts of the ramp are dominated by geothermal circulation. It is therefore inferred that the Kozár Limestone Member escaped early dolomitization because the refluxing brines could not reach the middle ramp shoal deposits (Fig. 13a).

5.2. Intermediate burial diagenesis

5.2.1. First dolomite recrystallization

Dolomites that form in near-surface environments from seawater or evaporitic brines are metastable, and therefore are prone to recrystallization due to increasing temperature and pressure during burial, and/or changing fluid composition (Land, 1985; Gregg and Shelton, 1990; Machel, 2004; Kaczmarek et al., 2017). The dolomites in Kán Dolomite Member fall into this category.

Reflux dolomitization of the Kán Dolomite is inferred from three aspects: the paleogeographic and paleoclimatic setting (peritidal environment and semiarid to semihumid climate), its sedimentological characteristics (e.g., teepee structures, evaporite pseudomorphs), and the $\delta^{18}O_{fluid}$ value of the fluid calculated from the clumped isotope data of the fine crystalline dolomites (2.0 to 3.0‰$_{V\text{-}SMOW}$). However, reflux dolomites typically have $\delta^{18}O_{dol}$ values around +4‰$_{V\text{-}PDB}$ (e.g., Land, 1985), whereas the $\delta^{18}O_{dol}$ values of the fine crystalline dolomites of the Mecsek Mts. are significantly lower (highest value is –1.9‰$_{V\text{-}PDB}$, Fig. 8, Table 2). This discrepancy between the measured and the expected values can be explained by significant recrystallization (*sensu* Machel 1997) of the reflux dolomites with respect to $\delta^{18}O_{dol}$. This notion is further supported by the clumped isotope data, which indicate elevated temperatures (50 to 67 °C) and mesohaline brines (2.0 to 3.0‰$_{V\text{-}SMOW}$) (Fig. 9). Such temperatures are too high for near-surface diagenetic settings (except for a few exceptionally hot playa settings) and thus are interpreted to represent an intermediate burial setting, corresponding to 1–2 km burial depth, as estimated from the clumped

isotope temperatures using a 25 to 30°C/km geothermal gradient. Based on the burial history of the area (Haas et al., 1995), the Kán Dolomite Member is estimated to have reached this burial depth and temperature range during the Early Jurassic (Fig. 13b). The driving force for recrystallization of the fine crystalline dolomites likely was increased temperature due to burial, possibly aided by a change in fluid composition and an additional temperature rise caused by geothermal circulation of the connate brines. The latter is suggested by the $\delta^{18}O_{dol}$ and Δ_{47} values of the Kán Dolomite, which were reset by water-rock interactions to now represent the environment of recrystallization, i.e., temperatures higher than that during dolomitization and a slightly modified $\delta^{18}O_{fluid}$ composition, while preserving the mesohaline $\delta^{18}O_{fluid}$ signature of the diagenetic fluids (connate brine) (Fig. 8, 9).

Recrystallization by meteoric fluids can also be the cause of the observed negative shift in the $\delta^{18}O_{dol}$ values. However, this process is excluded for the Kán Dolomite Member based on the calculated $\delta^{18}O_{fluid}$ values. Alternatively, the observed negative $\delta^{18}O_{dol}$ values can result from dolomitization during burial (as opposed to recrystallization of near-surface dolomites during burial). However, numerical modelling studies indicate that even though refluxing brines may advect down to significant depths (up to ~2 km, but only in the absence of effective aquitards; Jones et al., 2004), dolomitization is likely restricted to the uppermost part of the carbonate succession (2 to 3 m) because the Mg^{2+} available for dolomitization is rapidly exhausted (Jones et al., 2003). Therefore, we contend that the negative $\delta^{18}O_{dol}$ values of the fine crystalline dolomites are indeed the result of burial recrystallization in mesohaline connate fluids.

5.2.2. Gypsum dissolution and dolomite cementation

Synsedimentary gypsum that had formed during periods of increased salinity either was dissolved almost penecontemporaneously during periodic freshening of the pore fluids via latent reflux *sensu* Jones et al. (2003), or via thermally driven circulation during intermediate burial of the mesohaline pore waters that were likewise undersaturated with respect to gypsum. One or both alternatives left behind moldic pores in the fine crystalline dolomites. The available data do not provide sufficient evidence to decide between these two alternatives.

Increasing burial and related stylolitization may have periodically caused the pore fluids to become supersaturated with respect to dolomite due to the newly available Mg^{2+} that was liberated during pressure dissolution of the dolomite (cf., Wanless, 1979). The small amounts of planar dolomite cements that line or fill moldic pores in the fine crystalline dolomites (Fig. 3e–f), and the thin limpid dolomite overgrowth cements observed in the medium crystalline, planar-s dolomites with poorly preserved ooid-peloidal grainstone fabric (Fig. 4a), are thus interpreted to have likely formed as a by-product of pressure solution of the preexisting dolomites. The overlap and the lack of a well-defined boundary in the $\delta^{18}O_{dol}$ values between the very fine to fine crystalline and the medium to very coarse crystalline dolomites (Fig. 8) thereby likely reflects the mixing of the values from two populations of dolomite, which are intergrown and thus cannot be separated via microdrilling: the lower temperature (higher $\delta^{18}O_{dol}$) recrystallized matrix dolomites (see Section 5.2.1) and the higher temperature (lower $\delta^{18}O_{dol}$) cements. Alternatively, dolomite cementation might also have been related to the incursion of fluids with elevated temperature via fractures (see Section 5.3.1.), in which case the two dolomite phases in the powder mixtures would be dolomite cement precipitated from such fracture-related fluids and the earlier recrystallized matrix dolomite.

Further investigation using *in situ* secondary ion mass spectrometry (SIMS) is required to distinguish between these alternatives.

5.3. Deep burial diagenesis

5.3.1. High-temperature fault-controlled dolomitization and second recrystallization event

The irregular bodies of fabric destructive, coarse crystalline, planar-s to nonplanar-a dolomites with saddle dolomite cements that are present within the fine crystalline dolomites (Kán Dolomite) and in the coeval and underlying limestones (Kozár and Zuhánya Limestones, respectively) (Fig. 5–6) are interpreted to have formed in a deep burial setting from 'hot' fluids circulating through faults. These coarse crystalline dolomites have very low $\delta^{18}O_{dol}$ values (–15.4‰ $_{V\text{-}PDB}$ to –6.2‰$_{V\text{-}PDB}$) (Fig. 8), and the clumped isotope analysis yielded temperature of 107 to 130 °C for the parent fluid (Fig. 9). These data suggest that interaction of the rocks with these 'hot' fluids resulted in recrystallization of the pre-existing fine crystalline dolomites, and in the dolomitization of the previously undolomitized coeval Kozár and the underlying Zuhánya Limestones. Thus, parts of the Kán Dolomite Member appear to have been recrystallized for a second time, this time driven by the fault-derived 'hot' fluids.

The formation of some of these coarse crystalline dolomites was previously interpreted to have been related either to the Early Cretaceous submarine mafic igneous activity in the area (Wéber, 1978), or to the Late Cretaceous or Cenozoic thrusting (Nagy, 1968). However, no convincing evidence was provided by these studies to support the hypothesis of igneous activity-related dolomitization. The spatial proximity of mafic igneous intrusions to the coarse crystalline dolomites is no proof of a genetic relationship. Also, the Sr isotope values of the coarse crystalline dolomites are near or higher than that of Mesozoic seawater (Fig. 10), a trend opposite to what is expected from fluids that had interacted with mafic intrusions (cf. Burke et al., 1982; Banner,

1995). Therefore, the formation of the coarse crystalline dolomites from fluids related to Early Cretaceous igneous activity is not substantiated.

We propose that, as suggested by the Sr isotope data, the dolomitizing/recrystallizing agent was seawater, which was drawn down through a fault system that was created during the Early Cretaceous rifting (Fig. 13c). The medium to coarse crystalline dolomites fall into a narrow range and have slightly lower $^{87}Sr/^{86}Sr$ ratios (0.70780 to 0.70797) than that of the very fine to fine crystalline dolomites (0.70813 to 0.70819) and the undolomitized limestones (0.70798 to 0.70802) (Fig. 11, Table 2). This finding suggests that the dolomitizing and/or dolomite recrystallizing fluid had a Sr isotope composition lower than that of the precursor rocks. A candidate for such a fluid is Early Cretaceous seawater (Fig. 10). In this scenario, surface-breaching rift faults that were created related to the opening of the Vahic oceanic basin during the Early Cretaceous (cf., Haas and Péró, 2004) provided conduits for the descending seawater, which was heated either due to the regional geothermal heat or due to more localized heat of nearby igneous intrusions. Thermal convection was thus induced, and the hot fluids ascended along faults, thereby facilitating recrystallization of pre-existing fine crystalline dolomites for a second time in the vicinity of the faults. Where these hot fluids encountered the previously undolomitized middle ramp Kozár Limestone and the underlying Zuhánya Limestone, these limestones underwent extensive, pervasive dolomitization in the vicinity of the faults (Fig. 13c), with the amount of dolomite decreasing with increasing distance from the fluid source. The source of Mg^{2+} for this type of dolomitization thus was Cretaceous seawater, which had not lost its dolomitizing potential while descending [cf., mass balance calculations of Hirani et al. (2018) and reactive transport modelling results of Corbella et al. (2014) for similar scenarios]. The lesser amount of dolomite found in the Kozár Limestone at location MR is interpreted to be the result of its distal position from the major faults (not exposed) that transported the dolomitizing fluids. Based on the Sr isotope composition

and the calculated $\delta^{18}O_{fluid}$ values of the studied coarse crystalline dolomites in the Mecsek Mts. (Fig. 11), the diagenetic fluid is interpreted to have been a mixture of the connate fluids and the Early Cretaceous seawater that was drawn down through the faults. Similar scenarios were proposed to explain the dolomitization of Lower Cretaceous carbonates in southern Italy (Rustichelli et al., 2017) and in eastern Spain (Corbella et al., 2014). According to these studies, seawater was likely drawn down and circulated through a fault system that was created during the Cretaceous, thereby dolomitizing the rocks in the vicinity of the faults. Therefore, it seems possible that fault-controlled seawater dolomitization related to the Early Cretaceous rifting in the Tethyan realm was not uncommon. Similarly, Oligo–Miocene seawater drawn down and convected through rift related faults was interpreted to have been the dolomitizing fluid in Oligocene–Miocene carbonates in Borneo (Wilson et al., 2007) and in Eocene carbonates in Egypt (Hollis et al., 2017; Hirani et al., 2018).

5.3.2. Geothermal versus hydrothermal processes

By definition, hydrothermal dolomites are formed from fluids that are at least 5 to 10 °C warmer than the host rock (see Machel and Lonnee, 2002). To assess whether a dolomite can be considered hydrothermal or not, it is necessary to determine the temperature of the country rock relative to the diagenetic fluid at the time of dolomite formation. If the temperature of dolomite formation was higher than the maximum burial temperature of the surrounding rocks, then the dolomite was formed hydrothermally. If, however, the temperature of dolomite formation was lower than the maximum burial temperature, then this dolomite may or may not be hydrothermal, depending on when it formed during the burial history (Machel and Lonnee, 2002).

No precise estimates of maximum burial depth and associated maximum burial temperature are available for the Csukma Formation. However, its burial depth can be estimated to have been

around 5 km during the Early Cretaceous based on the burial history of the area (Haas et al., 1995). In addition, vitrinite reflectance values available on coal samples from the Lower Jurassic Mecsek Coal Formation (Fig. 2) can be used to estimate the maximum burial temperature of the Csukma Formation. The maximum burial temperature of the Mecsek Coal was determined to be 138 °C (Vető, 1978). The total thickness of the Kantavár and Karolinavölgy Formations (Fig. 2), which are situated between the Mecsek Coal and the Csukma Formations, is up to 720 m (thickness data from Török, 1998b). Using a conservative 25 °C/km geothermal gradient, this additional burial depth would correspond to ca. 156 °C maximum burial temperature of the studied dolomites. Based on clumped isotope measurements, the coarse crystalline dolomites were formed/recrystallized at temperatures 107 to 130 °C. Note, however, that the uncertainty of the methods (clumped isotope and vitrinite reflectance thermometry) together with the uncertainties of the estimates based on the burial history are beyond the 5 to 10 °C temperature range that is needed to differentiate between geothermal and hydrothermal processes. Nevertheless, the temperature of the dolomitizing fluid likely was not significantly, if at all, higher than the temperature of the surrounding rocks, if the dolomitization indeed occurred during the Early Cretaceous when these rocks were deeply buried. Therefore, these dolomites cannot be considered hydrothermal dolomites as defined by Machel and Lonnee (2002). However, in the area of the Northern Imbricates (Fig. 1b), where medium to coarse crystalline, planar-s to nonplanar-a dolomites with varied CL patterns occur (VA location, Figs. 1b, 4), the maximum burial temperature of the Mecsek Coal Formation was determined to be only 55 °C, and the coalification rank of the coal was only lignite before the emplacement of the igneous intrusions, which caused local coking of the lignite (Vető, 1978). Due to the different burial history of the Northern Imbricates compared to other parts of the Mecsek Mts. (Némedi Varga, 1995), the succession at location VA was not buried as deeply as those at the other studied locations. Using the above

calculation, the country rock temperature is estimated to have been around 73 °C, whereas the dolomitizing fluid at location VA was determined to be 130 °C based on clumped isotope measurement. Thus, the rocks at location VA were presumably significantly cooler than the dolomitizing fluid. Therefore, the coarse crystalline dolomites of the VA location are hydrothermal in origin as defined by Machel and Lonnee (2002). Furthermore, the $\delta^{18}O_{fluid}$ value calculated for a coarse crystalline dolomite from this location is significantly higher (4.3‰$_{V\text{-}SMOW}$) than that of the other coarse crystalline dolomites at other locations (1.3 to 2.6‰$_{V\text{-}SMOW}$) (Fig. 9), which suggests that the dolomitizing fluids at the VA location had a different source compared to the other locations in the Central and Western Mecsek (Fig. 1b), or these dolomites were later recrystallized in fluids related to a Late Cretaceous fluid flow event (see Section 5.3.3).

5.3.3. Saddle dolomite cementation

Saddle dolomite filling vugs and fractures within the medium to coarse crystalline, planar-s to nonplanar-a dolomites can be found at several locations (VA, AT, VP-2, HR), whereas saddle dolomite occurs only scarcely in the fine crystalline dolomites filling narrow fractures (e.g., in the VP-2 and GF-1 drill cores). The rather wide ranges in both the $\delta^{18}O_{dol}$ and $\delta^{13}C$ values of the saddle dolomite cements (Fig. 8, Table 2) likely indicate differences in the temperature of precipitation, and a difference in either the origin of the fluids or the fluid-to-rock ratio in the diagenetic system (e.g., Banner and Hanson, 1990). The saddle dolomites identified in the study area likely formed in two different ways: from seawater that was drawn down and circulated through the sequence along normal faults during the Early Cretaceous, and from basinal brines ascending along thrust faults during the Late Cretaceous or Cenozoic. Saddle dolomites with $\delta^{18}O_{dol}$ and $\delta^{13}C$ values close to the values of the country rock (e.g., at locations VP-2 and AT) (Table 2) may indicate a low

fluid-to-rock ratio and/or a long residence time of the fluids enabling near isotopic equilibration of the pore fluid with the host rock.

Based on the CL pattern of the saddle dolomites (Fig. 6), those with concentric growth zonation seem to have grown in multiple episodes or from fluids with changing composition. However, microdrilling cannot separate the observed growth zones. Therefore, stable isotope values measured on such samples are averages over the various growth zones. In addition to the concentric growth zonation within one set of saddle dolomite crystals filling a pore/fracture, there are samples with oscillatory zonation, which is a bulk solution disequilibrium phenomenon (Machel, 1990; Machel and Burton, 1991). Furthermore, changes in the chemistry or temperature of the diagenetic fluids along their flow paths may also cause variations in the CL pattern of time-equivalent cement generations (Machel and Burton, 1991). In this light, correlation of the various saddle dolomite types and/or growth zones is not possible within the study area. Again, *in situ* secondary ion mass spectrometric (SIMS) analysis of the isotopic composition of the various saddle dolomite types would help better characterize and correlate these cements.

The Sr isotope ratios of pairs of matrix dolomite and saddle dolomite from the same samples can be used to further characterize the fluid(s) of saddle dolomite formation. Such samples were analyzed from two locations (VA and AT, Fig. 1b) where the dolomites are interpreted to have been dolomitized for the first time by the high-temperature fluids (see Sections 5.3.1. and 5.3.2). In both cases, the Sr isotope ratios of the saddle dolomite cements are higher than that of the matrix dolomite (AT: 0.707940. and 0.70781, VA: 0.70823 and 0.70780, respectively) (Fig. 11), which indicate that the parent fluid of the saddle dolomite cement was more radiogenic (contained more radiogenic Sr) than the fluid that had caused the replacive matrix dolomitization. The more radiogenic Sr isotope composition of the saddle dolomite suggests a 'basinal' origin of the

precipitating fluids, i.e., fluids that were derived from either the Variscan crystalline basement rocks, or from late Paleozoic–early Mesozoic siliciclastic rocks (see Fig. 2).

The complex zonation and multiple generations of the saddle dolomite cements, therefore, likely reflect multiple episodes of saddle dolomite cementation, including precipitation from fluids derived from Cretaceous seawater, and repeated expulsion of basinal fluids during either the Late Cretaceous thrusting events and/or during the various thrusting events of the Miocene tectonic phases (cf. Csontos et al., 2002), even though correlations of these episodes is not possible from one location to another, as noted earlier. Such basinal fluid flow may have been responsible for resetting the $\delta^{18}O_{fluid}$ value of the dolomite at location VA, which is markedly different from the other studied dolomites. In southeast Hungary (Szeged Basin), hydrothermal alteration/recrystallization of the time-equivalent Szeged Dolomite was interpreted to have been caused by Late Cretaceous metamorphic fluids (Garaguly et al., 2018). Comparison of the Sr isotopic composition of the hydrothermal dolomites in the Szeged Basin with those in the Mecsek Mts. (Sr isotope ratios up to 0.709674 of the saddle dolomites in Szeged Dolomite according to Garaguly et al. (2018), compared to 0.70823 of the saddle dolomite at the VA location in the Mecsek Mts.) reveals that the hydrothermal fluids were of different origin. The Szeged Dolomite is part of the Békés-Codru Unit (nappe system), whereas the Csukma Formation belongs to the Mecsek Unit (nappe system); therefore, differences in the hydrothermal fluid sources are reasonable.

5.4. Post-dolomitization diagenesis

Even though only limited data are available to reconstruct the post-dolomitization diagenetic processes that affected the studied successions, an attempt was made to correlate the analyzed calcite cement phases to calcite cementation events known from the literature pertinent to the study

area, and to offer a possible explanation leading to the disintegration of some of the dolomites at location HR.

Petrographic and stable isotope data (Figs. 7 and 8) suggest that the late diagenetic calcites found within the studied dolomite successions were formed from fluids of two distinct sources, hydrothermal and meteoric. Based on the paragenetic sequence and the tectonic evolution of the area (Fig. 12), the calcite cementation occurred during uplift following maximum burial, i.e., in a telogenetic setting. Based on the $\delta^{18}O_{cal}$ and $\delta^{13}C$ values, three types of calcite cement can be differentiated, even though two of these are only represented by one sample each (Fig. 8). CAL-1 is a white, 'massive' fracture filling calcite sample from location VA with very low oxygen and relatively high carbon isotope values ($\delta^{18}O_{cal}$ –20.5‰; $\delta^{13}C$ –0.9‰). CAL-2 is a white, blocky calcite cement from a tectonic breccia from location GF-1 with less negative oxygen and similar carbon isotope values ($\delta^{18}O_{cal}$ –12.4‰; $\delta^{13}C$ –0.3‰). CAL-3 are three fracture and vug-filling calcite samples of brownish color from locations HR, RV and VP-2 with distinctly different isotope signature ($\delta^{18}O_{cal}$ –7.8 to –6.2‰; $\delta^{13}C$ –8.5 to –4.8‰) from the other two samples (CAL-1 and CAL-2).

At location VA, dolomitization and saddle dolomite cementation indicate that hydrothermal processes (section 5.3) preceded calcite cementation. While conclusive evidence is not available, it may well be that this calcite formed from the same hydrothermal fluid that had previously formed saddle dolomite at this location, and the fluid had evolved from dolomite formation to calcite formation over time, either due to cooling or to a change in composition (see Fig. 1 in Machel, 2004). Hydrothermal calcite veins are widespread in the Eastern Mecsek Mts. and Mórágy Hills (Fig. 1b) and the origin of these and the calcite vein at location VA (CAL-1) may be similar. The origin of the calcite veins found within Paleozoic crystalline rocks in these areas were linked to

hydrothermal processes either related to the Early Cretaceous igneous activity (Jáger et al., 2012; Dabi et al., 2013) or to hydrothermal fluid circulation during the Late Cretaceous (Poros et al., 2008). Based on the geological evolution of the Northern Imbricates (location VA, Fig.1b), the calcite cementation (CAL-1) was likely related to the Late Cretaceous hydrothermal fluid flow event (fluid flow event 3b of Poros et al., 2008).

On the other hand, the calcite cement from location GF-1 (CAL-2) (Fig. 1b) has an isotopic composition similar to calcite veins that occur in Permian siltstones in the Western Mecsek Mts. ($\delta^{18}O_{cal}$ –16 to –12‰$_{V\text{-}PDB}$, originally reported in V-SMOW, and $\delta^{13}C$ –5.5 to –0.2‰) (Demény and Fórizs, 1996). These calcites in the siltstones were determined to have precipitated from waters of meteoric origin during a period of warm climate before the Pleistocene on the basis of stable isotope and fluid inclusion studies (Demény and Fórizs, 1996). The similarity of the values and geological evolution of the area suggest that the calcite cement at location GF-1 (CAL-2) formed from the same or similar fluid, likely during the major inversion tectonic event during the Pliocene (cf. Csontos et al., 2002).

The $\delta^{18}O_{cal}$ and $\delta^{13}C$ values of the third group of calcite cements (CAL-3) is distinct from the other two and they fall near the more positive end of the range of values measured on speleothems ($\delta^{18}O$ –12.3 to –6.5; $\delta^{13}C$ –12.7 to –7.3) that precipitated during the last glacial period in a cave that formed in the Middle Triassic Lapis Limestone Formation (Fig. 2) in the Western Mecsek Mts. (Koltai et al., 2017). The similarity in the values indicate that the late fracture and vug filling calcites (CAL-3) of the current study likely precipitated from meteoric fluids during the Pleistocene. In addition to the climatic variation, the more positive $\delta^{18}O_{cal}$ and $\delta^{13}C$ values of the CAL-3 calcite cements may reflect the extent of the interaction between the meteoric fluid and the country rock and/or variable mixing proportions of the connate waters with the meteoric fluids.

The incursion of meteoric waters is further suggested by dedolomitization (replacement of dolomite by calcite, see Nader et al., 2008; Hauck et al. 2018) of some non-planar replacive dolomites within the dolomitic limestones (Fig. 5c), as well as by selective replacement of certain, likely originally iron-rich, zones of saddle dolomite cements (Fig. 6i). Calcite filled some stylolitic surfaces in the fine crystalline dolomites that likely opened up due to uplift related unloading. Even though it was not possible to determine the isotope composition of these minor calcite phases, the geological evolution of the area suggest their precipitation with the involvement of meteoric water. The isotope signature of the limestone samples (Fig. 8) may indicate meteoric recrystallization (neomorphism *sensu* Folk, 1965) or burial diagenesis. A detailed evaluation of the diagenetic evolution of the limestones is the subject of a forthcoming paper.

A peculiar feature within the coarse crystalline dolomites at location HR (Fig. 1b) is the occurrence of small (1–2 m thick/wide) irregular bodies of friable (disintegrating), coarse crystalline dolomites (Fig. 4e–f). The stable isotopic composition of these disintegrating dolomites is indistinguishable from that of the massive coarse crystalline dolomite within which they occur. Even though detailed chemical analysis of the disintegrating dolomites in the Mecsek Mts. has not been performed, the stable isotope data suggest that the process leading to the disintegration did not involve chemical alteration of the pre-existing dolomites, although chemical weathering processes cannot be ruled out. A more likely explanation for this phenomenon is 'cryogenic powderization' (repeated freezing-thawing cycles) as suggested by Poros et al. (2013) in the case of the Upper Triassic Fődolomit (Hauptdolomit/Dolomia Principale equivalent) in the Transdanubian Range, Hungary. Further assessment of the origin of the disintegrating dolomites is beyond the scope of the present study.

6. Conclusions

The peritidal–shallow marine carbonates of the Csukma Formation of the Mecsek Mts. underwent multiple phases of dolomitization, dolomite recrystallization and cementation. Integration of petrographic and geochemical data with paleogeography (e.g., Török, 1998a; Szulc, 2000) and tectonic evolution (e.g., Csontos et al., 2002; Haas and Péró, 2004) enabled a detailed interpretation of the diagenetic processes that affected the Csukma Formation.

The most important findings of this study are the following:

1. Integration of carbon, oxygen, strontium and clumped isotope data can help discriminate various diagenetic fluids and processes that are otherwise difficult to distinguish.
2. Extensive dolomitization of the Csukma Formation (Kán Dolomite Member) was primarily controlled by its paleogeographic setting (i.e., depositional environment and climatic conditions). The peritidal inner ramp carbonates likely were dolomitized by refluxing evaporatively concentrated brines, in agreement with earlier studies (e.g., Konrád, 1998; Török, 1998a). These reflux dolomites were significantly recrystallized with respect to $\delta^{18}O_{dolomite}$ in the presence of connate brines in an intermediate burial setting.
3. The coarse crystalline dolomites were formed in a deep burial setting as a result of dolomitization and recrystallization by high-temperature fluids. Such fluids were likely derived from Cretaceous seawater that was drawn down and circulated through rift-related faults. This study, therefore, provides a new example for fault-controlled seawater dolomitization occurring in extensional basins.

Acknowledgements

This work was supported by the American Association of Petroleum Geologists Grants-in-Aid Program, the Geological Society of America Graduate Student Research Grant Program, the International Association of Sedimentologists Post-Graduate Grant Scheme, and the Hungarian Scientific Research Fund (OTKA K124313). SK was supported by the National Research, Development and Innovation Office (NKFIH, KH 125584). The authors are indebted to Tamás Budai and Gyula Konrád for their continued help and support, and to Mecsekérc Ltd. for providing access to the VP-2 drill cores. The comments and suggestions of Alessandro Iannace and an anonymous reviewer are greatly appreciated.

References

Adams, A., Diamond, L.W. and Aschwanden, L., 2018. Dolomitization by hypersaline reflux into dense groundwaters as revealed by vertical trends in strontium and oxygen isotopes: Upper Muschelkalk, Switzerland. Sedimentology.

Al-Aasm, I.S. and Packard, J.J., 2000. Stabilization of early–formed dolomite: a tale of divergence from two Mississippian dolomites. Sedimentary Geology, 131(3–4): 97–108.

Banner, J.L., 1995. Application of the trace element and isotope geochemistry of strontium to studies of carbonate diagenesis. Sedimentology, 42(5): 805–824.

Banner, J.L., Hanson, G. and Meyers, W., 1988. Water-rock interaction history of regionally extensive dolomites of the Burlington-Keokuk Formation (Mississippian): isotopic evidence.

Banner, J.L. and Hanson, G.N., 1990. Calculation of simultaneous isotopic and trace element variations during water-rock interaction with applications to carbonate diagenesis. Geochimica et Cosmochimica Acta, 54(11): 3123–3137.

Bellieni, G., Fioretti, A., Marzoli, A. and Visonà, D., 2010. Permo–Paleogene magmatism in the eastern Alps. Rendiconti Lincei, 21(1): 51–71.

Bilik, I., 1980. Lower Cretaceous submarine (rift) volcanism in South Transdanubia (South Hungary). In: E. Bisztricsány and G. Szeidovitz (Editors), Proceedings of the 17th Assembly of the European Seismological Congress. Akadémiai Kiadó, Budapest.

Bleahu, M., Mantea, G., Bordea, S., Panin, S., Stefanescu, M., Sikic, K., Haas, J., Kovács, S., Péró, C. and Bérczi-Makk, A., 1994. Triassic facies types, evolution and paleogeographic relations of the Tisza Megaunit. Acta Geologica Hungarica, 37(3–4): 187–234.

Bonifacie, M., Calmels, D., Eiler, J.M., Horita, J., Chaduteau, C., Vasconcelos, C., Agrinier, P., Katz, A., Passey, B.H. and Ferry, J.M., 2017. Calibration of the dolomite clumped isotope thermometer from 25 to 350° C, and implications for a universal calibration for all (Ca, Mg, Fe) CO_3 carbonates. Geochimica et Cosmochimica Acta, 200: 255–279.

Budai, T., Haas, J., Konrád, G. and Koroknai, B., 2014. Tisza Mega-unit. In: J. Haas and T. Budai (Editors), Geology of the pre-Cenozoic basement of Hungary. Explanatory notes for "Pre-Cenozoic geological map of Hungary" (1:500 000). Geological and Geophysical Institute of Hungary, Budapest.

Burke, W., Denison, R., Hetherington, E., Koepnick, R., Nelson, H. and Otto, J., 1982. Variation of seawater $^{87}Sr/^{86}Sr$ throughout Phanerozoic time. Geology, 10(10): 516–519.

Came, R.E., Azmy, K., Tripati, A. and Olanipekun, B.J., 2017. Comparison of clumped isotope signatures of dolomite cements to fluid inclusion thermometry in the temperature range of 73–176°C. Geochimica et Cosmochimica Acta, 199: 31–47.

Corbella, M., Gomez-Rivas, E., Martín-Martín, J.D., Stafford, S., Teixell, A., Griera, A., Travé, A., Cardellach, E. and Salas, R., 2014. Insights to controls on dolomitization by means of reactive transport models applied to the Benicàssim case study (Maestrat Basin, eastern Spain). Petroleum Geoscience, 20(1): 41–54.

Császár, G., 1998. Lower and Middle Cretaceous stratigraphy of the Mecsek-Villány unit. In: I. Bérczi and Á. Jámbor (Editors), Stratigraphy of the geological formations of Hungary. MOL-MÁFI, Budapest, pp. 353–370.

Csontos, L., Benkovics, L., Bergerat, F., Mansy, J.L. and Wórum, G., 2002. Tertiary deformation history from seismic section study and fault analysis in a former European Tethyan margin (the Mecsek–Villány area, SW Hungary). Tectonophysics, 357(1): 81–102.

Csontos, L., Nagymarosy, A., Horváth, F. and Kovác, M., 1992. Tertiary evolution of the Intra-Carpathian area: A model. Tectonophysics, 208(1): 221–241.

Dabi, G., Bajnóczi, B., Schubert, F. and M. Tóth, T., 2013. The origin and role of a calcite-filled microcrack generation in a metamorphic crystalline complex: The characterization of a fossilised seismic permeability system. Tectonophysics, 608: 792–803.

Dale, A., John, C.M., Mozley, P.S., Smalley, P.C. and Muggeridge, A.H., 2014. Time-capsule concretions: Unlocking burial diagenetic processes in the Mancos Shale using carbonate clumped isotopes. Earth and Planetary Science Letters, 394(Supplement C): 30–37.

Davies, A.J. and John, C.M., 2018. The clumped (^{13}C–^{18}O) isotope composition of echinoid calcite: further evidence for “vital effects” in the clumped isotope proxy. Geochimica et Cosmochimica Acta. doi: https://doi.org/10.1016/j.gca.2018.07.038

Demény, A., Fórizs, I. and Máthé, Z., 1996. A Preliminary Stable Isotope Study on a Potential Radioactive Waste Repository Site in the Mecsek Mountains, Southern Hungary. Rapid Communications in Mass Spectrometry, 10(11): 1415–1417.

Dickson, J., 1966. Carbonate identification and genesis as revealed by staining. Journal of Sedimentary Research, 36(2).

Durocher, S. and Al–Aasm, I.S., 1997. Dolomitization and neomorphism of Mississippian (Visean) upper Debolt Formation, Blueberry Field, northeastern British Columbia: geologic, petrologic, and chemical evidence. AAPG bulletin, 81(6): 954–977.

Eiler, J.M., 2007. "Clumped-isotope" geochemistry—The study of naturally-occurring, multiply-substituted isotopologues. Earth and Planetary Science Letters, 262(3–4): 309–327.

Esteban, M., Budai, T., Juhász, E. and Lapointe, P., 2009. Alteration of Triassic carbonates in the Buda Mountains—a hydrothermal model. Central European Geology, 52(1): 1–29.

Feist-Burkhardt, S., Götz, A.E., Szulc, J., Borkhataria, R., Geluk, M., Haas, J., Hornung, J., Jordan, P., Kempf, O. and Michalík, J., 2008. Triassic. The geology of central Europe, 2: 749–821.

Ferry, J.M., Passey, B.H., Vasconcelos, C. and Eiler, J.M., 2011. Formation of dolomite at 40–80 °C in the Latemar carbonate buildup, Dolomites, Italy, from clumped isotope thermometry. Geology, 39(6): 571–574.

Folk, R.L., 1959. Practical petrographic classification of limestones. AAPG Bulletin, 43(1): 1–38.

Folk, R.L., 1965. Some aspects of recrystallization in ancient limestones. In: L.C. Pray and R.C. Murray (Editors), Dolomitization and Limestone Diagenesis. SEPM, Tulsa, pp. 14–48.

Friedman, I. and O'Neil, J.R., 1977. Data of geochemistry: Compilation of stable isotope fractionation factors of geochemical interest, 440. US Government Printing Office. KK1–KK12

Garaguly, I., Varga, A., Raucsik, B., Schubert, F., Czuppon, G. and Frei, R., 2018. Pervasive early diagenetic dolomitization, subsequent hydrothermal alteration, and late stage hydrocarbon accumulation in a Middle Triassic carbonate sequence (Szeged Basin, SE Hungary). Marine and Petroleum Geology, 98: 270–290.

Gat, J.R. and Gat, J.R., 1978. Isotope hydrology of inland sabkhas in the Bardawil area, Sinai. Limnology and Oceanography, 23(5): 841–850.

Ghosh, P., Adkins, J., Affek, H., Balta, B., Guo, W., Schauble, E.A., Schrag, D. and Eiler, J.M., 2006. 13C–18O bonds in carbonate minerals: A new kind of paleothermometer. Geochimica et Cosmochimica Acta, 70(6): 1439–1456.

Götz, A.E., Török, Á., Feist-Burkhardt, S. and Konrád, G., 2003. Palynofacies patterns of Middle Triassic ramp deposits (Mecsek Mts., S Hungary): a powerful tool for high-resolution sequence stratigraphy. Mitt. Ges. Geol. Bergbaustud. Österr, 46: 77–90.

Götz, A.E. and Török, Á., 2008. Correlation of Tethyan and Peri–Tethyan long–term and high–frequency eustatic signals (Anisian, Middle Triassic). Geologica Carpathica, 59(4): 307–317.

Gregg, J.M., Bish, D.L., Kaczmarek, S.E. and Machel, H.G., 2015. Mineralogy, nucleation and growth of dolomite in the laboratory and sedimentary environment: A review. Sedimentology, 62(6): 1749–1769.

Gregg, J.M., Howard, S.A. and Mazzullo, S., 1992. Early diagenetic recrystallization of Holocene (< 3000 years old) peritidal dolomites, Ambergris Cay, Belize. Sedimentology, 39(1): 143–160.

Gregg, J.M. and Shelton, K.L., 1990. Dolomitization and dolomite neomorphism in the back reef facies of the Bonneterre and Davis formations (Cambrian), southeastern Missouri. Journal of Sedimentary Research, 60(4).

Haas, J., 2012. Geology of Hungary. Springer Science & Business Media. 244 p.

Haas, J., Budai, T., Hips, K., Konrád, G. and Török, Á., 2002. Sequence stratigraphy of Triassic facies areas in Hungary. Földtani Közlöny, 132(1): 17–43.

Haas, J., Budai, T. and Raucsik, B., 2012. Climatic controls on sedimentary environments in the Triassic of the Transdanubian Range (Western Hungary). Paleogeography, Paleoclimatology, Paleoecology, 353: 31–44.

Haas, J., Hips, K., Budai, T., Győri, O., Lukoczki, G., Kele, S., Demény, A. and Poros, Z., 2017. Processes and controlling factors of polygenetic dolomite formation in the Transdanubian Range, Hungary: a synopsis. International Journal of Earth Sciences, 106(3): 991–1021.

Haas, J., Kovács, S. and Török, Á., 1995. Early Alpine Shelf Evolution in the Hungarian Segments of the Tethys Margin. Acta Geologica Hungarica, 38(2): 95–110.

Haas, J. and Péró, C., 2004. Mesozoic evolution of the Tisza Mega–unit. International Journal of Earth Sciences, 93(2): 297–313.

Harangi, S., Szabó, C., Józsa, S., Szoldán, Z., Árva-Śos, E., Balla, M. and Kubovics, I., 1996. Mesozoic igneous suites in Hungary: Implications for genesis and tectonic setting in the northwestern part of Tethys. International Geology Review, 38(4): 336–360.

Hardie, L.A., 1987. Dolomitization; a critical view of some current views. Journal of Sedimentary Research, 57(1): 166–183.

Hauck, T.E., Corlett, H.J., Grobe, M., Walton, E.L. and Sansjofre, P., 2018. Meteoric diagenesis and dedolomite fabrics in precursor primary dolomicrite in a mixed carbonate–evaporite system. Sedimentology, 65(6): 1827–1858.

Hirani, J., Bastesen, E., Boyce, A., Corlett, H., Gawthorpe, R., Hollis, C., John, C.M., Robertson, H., Rotevatn, A. and Whitaker, F., 2018. Controls on the formation of stratabound dolostone bodies, Hammam Faraun Fault block, Gulf of Suez. Sedimentology, 65(6): 1973–2002.

Hollis, C., Bastesen, E., Boyce, A., Corlett, H., Gawthorpe, R., Hirani, J., Rotevatn, A. and Whitaker, F., 2017. Fault–controlled dolomitization in a rift basin. Geology, 45(3): 219–222.

Honlet, R., Gasparrini, M., Muchez, P., Swennen, R. and John, Cédric M., 2018. A new approach to geobarometry by combining fluid inclusion and clumped isotope thermometry in hydrothermal carbonates. Terra Nova, 30(3): 199–206.

Horita, J., 2014. Oxygen and carbon isotope fractionation in the system dolomite–water–CO_2 to elevated temperatures. Geochimica et Cosmochimica Acta, 129: 111–124.

Jáger, V., Molnár, F., Buchs, D. and Koděra, P., 2012. The connection between iron ore formations and "mud-shrimp" colonizations around sunken wood debris and hydrothermal sediments in a Lower Cretaceous continental rift basin, Mecsek Mts., Hungary. Earth-Science Reviews, 114(3): 250–278.

Jáger, V., 2015. Hydrothermal processes and ore indication related to the Early Cretaceous volcanism in the Eastern Mecsek Mts., PhD Dissertation, Eötvös Loránd University, Budapest, 164 p.

Jones, G.D., Smart, P.L., Whitaker, F.F., Rostron, B.J. and Machel, H.G., 2003. Numerical modeling of reflux dolomitization in the Grosmont platform complex (Upper Devonian), Western Canada sedimentary basin. AAPG bulletin, 87(8): 1273–1298.

Jones, G.D., Whitaker, F.F., Smart, P.L. and Sanford, W.E., 2004. Numerical analysis of seawater circulation in carbonate platforms: II. The dynamic interaction between geothermal and brine reflux circulation. American Journal of Science, 304(3): 250–284.

Kaczmarek, S.E., Gregg, J.M., Bish, D.L., Machel, H.G. and Fouke, B.W., 2018. Dolomite, Very High–Magnesium Calcite, and Microbes—Implications for the Microbial Model of Dolomitization. In: A.J. MacNeil, J. Lonnee and R. Wood (Editors), Characterization and

Modeling of Carbonates – Mountjoy Symposium 1. Special Publication. SEPM, Tulsa, pp. 7–20.

Kaczmarek, S.E. and Sibley, D.F., 2011. On the evolution of dolomite stoichiometry and cation order during high–temperature synthesis experiments: An alternative model for the geochemical evolution of natural dolomites. Sedimentary Geology, 240(1): 30–40.

Koltai, G., Spötl, C., Shen, C.C., Wu, C.C., Rao, Z., Palcsu, L., Kele, S., Surányi, G. and Bárány-Kevei, I., 2017. A penultimate glacial climate record from southern Hungary. Journal of Quaternary Science, 32(7): 946–956.

Konrád, G., 1998. Synsedimentary tectonic events in the Middle Triassic evolution of the SE Transdanubian part of the Tisza Unit. Acta Geologica Hungarica, 41(3): 327–341.

Korte, C., Kozur, H.W., Bruckschen, P. and Veizer, J., 2003. Strontium isotope evolution of Late Permian and Triassic seawater. Geochimica et Cosmochimica Acta, 67(1): 47–62.

Kupecz, J. and Land, L., 1994. Progressive recrystallization and stabilization of early–stage dolomite: Lower Ordovician Ellenburger Group, west Texas. Dolomites: A volume in Honour of Dolomieu. B. Purser, M., Tucker, D. Zenger (eds.). International Association of Sedimentology Special Publication (21): 255–279.

Land, L.S., 1980. The Isotopic and Trace Element Geochemistry of Dolomite: The State of the Art. In: D.H. Zenger, J.B. Dunham and R.L. Ethington (Editors), Concepts and Models of Dolomitization. SEPM Special Publication (28): 87–110.

Land, L.S., 1985. The origin of massive dolomite. Journal of Geological Education, 33(2): 112–125.

Lawson, M., Shenton, B.J., Stolper, D.A., Eiler, J.M., Rasbury, E.T., Becker, T.P., Phillips-Lander, C.M., Buono, A.S., Becker, S.P., Pottorf, R., Gray, G.G., Yurewicz, D. and Gournay, J., 2018. Deciphering the diagenetic history of the El Abra Formation of eastern

Mexico using reordered clumped isotope temperatures and U-Pb dating. GSA Bulletin, 130(3-4): 617–629.

Lohmann, K.C., 1988. Geochemical Patterns of Meteoric Diagenetic Systems and Their Application to Studies of Paleokarst. In: N.P. James and P.W. Choquette (Editors), Paleokarst. Springer New York, New York, NY, pp. 58–80.

Lonnee, J. and Machel, H.G., 2006. Pervasive dolomitization with subsequent hydrothermal alteration in the Clarke Lake gas field, Middle Devonian Slave Point Formation, British Columbia, Canada. AAPG bulletin, 90(11): 1739–1761.

Loyd, S.J., Corsetti, F.A., Eagle, R.A., Hagadorn, J.W., Shen, Y., Zhang, X., Bonifacie, M. and Tripati, A.K., 2015. Evolution of Neoproterozoic Wonoka–Shuram Anomaly-aged carbonates: Evidence from clumped isotope paleothermometry. Precambrian Research, 264: 179–191.

Lukoczki, G., Budai, T. and Németh, T., 2015. Sideritic-kaolinitic and green clay layers in the Mecsek Mountains (SW Hungary): Indicators of Middle Triassic volcanism—Myth or reality? Central European Geology, 58(4): 334–355.

MacDonald, J.M., John, C.M. and Girard, J.-P., 2018. Testing clumped isotopes as a reservoir characterization tool: a comparison with fluid inclusions in a dolomitized sedimentary carbonate reservoir buried to 2–4 km. Geological Society, London, Special Publications, 468: 189–202.

Machel, H.G., 1990. Bulk solution disequilibrium in aqueous fluids as exemplified by diagenetic carbonates. In: I.D. Meshri and P.J. Ortoleva (Editors), Prediction of Reservoir Quality through Chemical Modeling. AAPG, Tulsa, pp. 71–83.

Machel, H.G., 1997. Recrystallization versus neomorphism, and the concept of 'significant recrystallization' in dolomite research. Sedimentary Geology, 113(3): 161–168.

Machel, H.G., 1999. Effects of groundwater flow on mineral diagenesis, with emphasis on carbonate aquifers. Hydrogeology Journal, 7(1): 94–107.

Machel, H.G., 2004. Concepts and models of dolomitization: a critical reappraisal. Geological Society, London, Special Publications, 235(1): 7–63.

Machel, H.G. and Burton, E.A., 1991. Factors governing cathodoluminescence in calcite and dolomite, and their implications for studies of carbonate diagenesis. In: C.E. Barker and O.C. Kopp (Editors), Luminescence Microscopy: Quantitative and Qualitative Aspects. SEPM, Tulsa, pp. 37–58.

Machel, H.G. and Buschkuehle, B.E., 2008. Diagenesis of the Devonian Southesk–Cairn Carbonate Complex, Alberta, Canada: marine cementation, burial dolomitization, thermochemical sulfate reduction, anhydritization, and squeegee fluid flow. Journal of Sedimentary Research, 78(5): 366–389.

Machel, H.G., Cavell, P.A. and Patey, K.S., 1996. Isotopic evidence for carbonate cementation and recrystallization, and for tectonic expulsion of fluids into the Western Canada Sedimentary Basin. GSA Bulletin, 108(9): 1108–1119.

Machel, H.G. and Lonnee, J., 2002. Hydrothermal dolomite—A product of poor definition and imagination. Sedimentary geology, 152(3): 163–171.

Magyar, I., Geary, D.H. and Müller, P., 1999. Paleogeographic evolution of the Late Miocene Lake Pannon in Central Europe. Paleogeography, Paleoclimatology, Paleoecology, 147(3): 151–167.

Major, R., Lloyd, R.M. and Lucia, F.J., 1992. Oxygen isotope composition of Holocene dolomite formed in a humid hypersaline setting. Geology, 20(7): 586–588.

Mangenot, X., Gasparrini, M., Rouchon, V. and Bonifacie, M., 2018. Basin-scale thermal and fluid flow histories revealed by carbonate clumped isotopes (Δ_{47}) – Middle Jurassic carbonates of the Paris Basin depocentre. Sedimentology, 65(1): 123–150.

Mazzullo, S.J., 1992. Geochemical and neomorphic alteration of dolomite: A review. Carbonates and Evaporites, 7(1): 21–37.

McArthur, J.M., Howarth, R.J. and Shields, G.A., 2012. Strontium isotope stratigraphy. In: F.M. Gradstein, J.G. Ogg, M. Schmitz and G. Ogg (Editors), The geologic time scale. Elsevier, pp. 127–144.

McKenzie, J.A., 1981. Holocene dolomitization of calcium carbonate sediments from the coastal sabkhas of Abu Dhabi, UAE: a stable isotope study. The Journal of Geology, 89(2): 185–198.

Millán, I.M., Machel, H. and Bernasconi, S.M., 2016. Constraining temperatures of formation and composition of dolomitizing fluids in the Upper Devonian Nisku Formation (Alberta, Canada) with clumped isotopes. Journal of Sedimentary Research, 86(1): 107–112.

Montanez, I.P. and Read, J.F., 1992. Fluid–rock interaction history during stabilization of early dolomites, upper Knox Group (Lower Ordovician), US Appalachians. Journal of Sedimentary Research, 62(5).

Nader, F.H., Swennen, R. and Ellam, R., 2004. Reflux stratabound dolostone and hydrothermal volcanism–associated dolostone: a two-stage dolomitization model (Jurassic, Lebanon). Sedimentology, 51(2): 339–360.

Nader, F.H., Swennen, R. and Keppens, E., 2008. Calcitization/dedolomitization of Jurassic dolostones (Lebanon): results from petrographic and sequential geochemical analyses. Sedimentology, 55(5): 1467–1485.

Nagy, E., 1968. The Triassic of the Mecsek Mountains. Annals of the Hungarian Geological Institute, 51, Budapest.

Némedi Varga, Z., 1983. Tectonics of the Mecsek Mountains in the Alpine orogenic cycle, Annual Report of the Hungarian Geological Institute from 1981, 467–484.

Némedi Varga, Z., 1995. The research history and economic geology of the bituminous coal in the Mecsek Mts. University of Miskolc, Miskolc, Hungary, 472 p.

Némedi Varga, Z., 1998. Jurassic stratigraphy of the Mecsek-Villány unit. In: I. Bérczi and Á. Jámbor (Editor), Stratigraphy of the geological formations of Hungary. MOL-MÁFI, Budapest, 319–336.

Poros, Z., Molnár, F., Koroknai, B., Lespinasse, M., Maros, G. and Benkó, Z., 2008. Application of studies on fluid inclusion planes and fracture systems in the reconstruction of the fracturing history of granitoid rocks III: Results of studies in drillcores from the radioactive waste depository site at Bátaapáti (Üveghuta). Földtani Közlöny, 138(4): 363–384.

Poros, Z., Machel, H.G., Mindszenty, A. and Molnár, F., 2013. Cryogenic powderization of Triassic dolostones in the Buda Hills, Hungary. International Journal of Earth Sciences, 102(5): 1513–1539.

Qing, H. and Mountjoy, E.W., 1994. Rare earth element geochemistry of dolomites in the Middle Devonian Presqu'ile barrier, Western Canada Sedimentary Basin: implications for fluid-rock ratios during dolomitization. Sedimentology, 41(4): 787–804.

Rustichelli, A., Iannace, A., Tondi, E., Di Celma, C., Cilona, A., Giorgioni, M., Parente, M., Girundo, M. and Invernizzi, C., 2017. Fault-controlled dolomite bodies as palaeotectonic indicators and geofluid reservoirs: New insights from Gargano Promontory outcrops. Sedimentology, 64(7): 1871–1900.

Sena, C.M., John, C.M., Jourdan, A.-L., Vandeginste, V. and Manning, C., 2014. Dolomitization of Lower Cretaceous Peritidal Carbonates By Modified Seawater: Constraints From Clumped Isotopic Paleothermometry, Elemental Chemistry, and Strontium Isotopes. Journal of Sedimentary Research, 84(7): 552–566.

Sibley, D.F. and Gregg, J.M., 1987. Classification of dolomite rock textures. Journal of Sedimentary Research, 57(6): 967–975.

Spötl, C. and Burns, S.J., 1991. Formation of 18O-depleted dolomite within a marine evaporitic sequence, Triassic Reichenhall Formation, Austria. Sedimentology, 38(6): 1041–1057.

Szulc, J., 2000. Middle Triassic evolution of the northern Peri–Tethys area as influenced by early opening of the Tethys Ocean, Annales Societatis Geologorum Poloniae, 1–48.

Török, Á., 1998a. Controls on development of Mid–Triassic ramps: examples from southern Hungary. Geological Society, London, Special Publications, 149(1): 339–367.

Török, Á., 1998b. Triassic stratigraphy of the Mecsek–Villány unit. In: I. Bérczi and Á. Jámbor (Editors), Stratigraphy of the geological formations of Hungary. MOL–MÁFI, Budapest, pp. 253–280.

Török, Á., 2000a. Muschelkalk carbonates in southern Hungary: an overview and comparison to German Muschelkalk. Zbl. Geol. Paläont. Teil I(9–10): 1085–1103.

Török, Á., 2000b. Formation of dolomite mottling in Middle Triassic ramp carbonates (Southern Hungary). Sedimentary Geology, 131(3): 131–145.

Vető, I., 1978. Reconstruction of the thermal genesis of dispersed hydrocarbons. Application of the method in the Hungarian hydrocarbon research. PhD Dissertation, Hungarian Academy of Sciences, Budapest, 66 p.

Viczián, I., 1995. Clay minerals in Mesozoic and Paleogene sedimentary rocks of Hungary. Romanian Journal of Mineralogy, 77: 35–44.

Wanless, H.R., 1979. Limestone response to stress; pressure solution and dolomitization. Journal of Sedimentary Research, 49(2): 437–462.

Wéber, B., 1978. Neuer Beitrag zur Kenntnis der anisischen und ladinischen Schichten des Mecsek–Gebirges. Földtani Közlöny, 108: 137–148.

Wéber, B., 1982. On the Neogene and Paleogene of the Mecsekalja Graben (S Hungary). Földtani Közlöny, 112(3): 209–240.

Wilson, M.E.J., Evans, M.J., Oxtoby, N.H., Nas, D.S., Donnelly, T. and Thirlwall, M., 2007. Reservoir quality, textural evolution, and origin of fault-associated dolomites. AAPG Bulletin, 91(9): 1247–1272.

Wright, W.R., 2001. Dolomitization, fluid–flow and mineralization of the Lower Carboniferous rocks of the Irish Midlands and Dublin Basin, University College Dublin, Belfield, Ireland.

Table captions

Table 1: Description of sampling locations with abbreviations (Location ID) used throughout the text.

Table 2: List of geochemical analytical results. CAL: calcite cement, LMST: limestone, MC: medium to coarse crystalline matrix dolomite, SD: saddle dolomite, VF: very fine to fine crystalline matrix dolomite.

Figure captions

Fig. 1: Location of the study area. **(a)** The study area is situated in SW Hungary as indicated by the red rectangle. The purple line is the Mid-Hungarian Fault Zone. The green lines mark the boundaries between the subunits of the Tisza Mega-Unit. MU: Mecsek Unit, VBU: Villány-Bihor Unit, BCU: Békés-Codru Unit (modified after Csontos et al., 1992). Grey shading indicates outcrops of Pre-Neogene formations (VH: Villány Hills). The inset shows the location of the Pannonian Basin and Hungary within Europe. **(b)** Simplified geological map of the study area showing the sampling locations (Cenozoic cover not shown). Shaded areas indicate outcrops of Pre-Cenozoic formations (modified after Haas, 2012). AT: Árpád-tető, GF-1: Gálosfa-1, HR: Hetvehely road-cut, MR: Misina road-cut, RV: Rák Valley, VA: Váralja quarry, VP-2: Vágotpuszta-2. Legend: 1: Upper Cretaceous continental and marine formations, 2: Lower Cretaceous volcanic rocks, 3: Middle Jurassic to Lower Cretaceous pelagic limestones, 4: Lower and Middle Jurassic siliciclastic formations, 5: Upper Triassic to Lower Jurassic coal-bearing siliciclastic formations, 6: Middle Triassic shallow marine siliciclastic and carbonate formations, 7: Lower Triassic siliciclastic formations, 8: Mesozoic rocks in general, 9: Permian and Upper Carboniferous continental siliciclastic formations, 10: Paleozoic crystalline rocks, 11: Mesozoic fault lines, 12: Cenozoic fault lines.

Fig. 2: Simplified stratigraphic column of the area of the Mecsek Mts. with emphasis on the Middle and Upper Triassic formations. The names of the studied formations are highlighted in bold (after Haas, 2012).

Fig. 3: Sedimentary and petrographic features of the fine to very fine crystalline dolomites. **(a)** Hand specimen of a very fine crystalline laminated dolomite. Yellow lines highlight curved lamination of uncertain origin. (Location HR) **(b)** Outcrop photograph of a teepee structure in

very fine crystalline dolomite. (Location RV) **(c)** Photomicrograph of quartz pseudomorphs after gypsum encased in very fine crystalline dolomite. Plane-polarized light. (Location GF-1) **(d)** Hand specimen of very fine crystalline dolomite containing molds filled with planar dolomite. (Location HR) **(e)** Photomicrograph of very fine crystalline dolomite with dolomite-filled molds. Plane-polarized light. (Location HR) **(f)** CL image of (e) showing CL zonation of the dolomite cement.

Fig. 4: Petrographic features of the medium to very coarse crystalline dolomites. **(a)** Photomicrograph of a medium crystalline, planar-s dolomite with micritic ghosts likely indicating an ooid grainstone/packstone precursor. (Location HR) **(b)** Photomicrograph of medium crystalline dolomite with cloudy core–clear rim fabric. Plane-polarized light. (Location AT) **(c)** CL image of (b) showing the mottled core and zoned rims corresponding to the cloudy cores and clear rims, respectively. **(d)** Photomicrograph of a coarse crystalline, planar-s dolomite. Yellow arrows point to intercrystal pores. Plane-polarized light. (Location HR) **(e)** Outcrop photograph of coarse crystalline friable dolomite. Yellow arrows point to vug-filling saddle dolomite more resistant to disintegration. (Location HR) **(f)** Photomicrograph of grain mount of nonplanar dolomite crystals of the friable coarse crystalline dolomite. Plain polarized light. (Location HR) **(g)** Hand specimen of a fine to coarse crystalline dolomite with bioclastic floatstone fabric. (Location VA) **(h)** Photomicrograph of an echinoid fragment within a fine to medium crystalline planar-s to nonplanar dolomite. Cross-polarized light. (Location VA) **(i)** CL image of (h) revealing textural difference between the finer crystalline dolomite (very dull) and the coarser crystalline dolomite (brighter red, zoned or mottled CL pattern).

Fig. 5: Petrographic features of the dolomitic limestones. **(a)** Outcrop photograph of dark grey mudstone with ochre replacive dolomite along joints and fractures (yellow arrows). (Location AT) **(b)** Photomicrograph of fine to medium crystalline, nonplanar to planar-s dolomite (dol) partially replacing a mudstone (pink, lmst). Stained thin section, plane-polarized light. (Location AT) **(c)** Photomicrograph of calcite pseudomorphs after dolomite (dedolomite) within a bioclastic grainstone. Original dolomite mineralogy is inferred based on the dark, likely iron hydroxide-bearing zones mimicking the shape of dolomite crystals. Some of these zones are highlighted by yellow lines. Stained thin section. Plane-polarized light. (Location MR) **(d)** Photomicrograph of a dolomitic limestone. Bivalve (?) shell fragments are non-mimetically replaced by medium to coarse crystalline nonplanar dolomite (dol). Plane-polarized light. Right side of the thin section is stained. (Location HR)

Fig. 6: Petrographic features representing a variety in saddle dolomite cements as found across the studied sedimentary succession. The numbers indicate paragenetic sequence within a given sample and do not correlate across samples. **(a)** Saddle dolomite cement with inclusion-rich zones (sd1) or clear (sd2) overgrowth filling a vug in coarse crystalline planar-s to nonplanar-a matrix dolomite (md). Final cement in the pore is calcite (cal). Plane-polarized light. (Location GF-1) **(b)** CL image of (a). The first saddle dolomite (sd1) with dull, mottled CL is cross-cut (arrow) and overgrown by a later saddle dolomite phase (sd2) with duller CL. The calcite (cal) displays complex bright and dull orange CL zonation. **(c)** Saddle dolomite cement (sd) filling a vug in very fine crystalline matrix dolomite (md). **(d)** CL image of (c). The saddle dolomite cement displays bright red concentric CL zonation. The final dolomite phase is nonluminescent. (Location GF-1) **(e)** Fracture-filling saddle dolomite cement. (Location VP-2) **(f)** CL image of (e). The saddle dolomite cement displays simple concentric and oscillatory concentric zonation.

Non-luminescent matrix dolomite (md) is overgrown by non-luminescent to bright red planar-c dolomite cement (cd). The first generation of saddle dolomite (sd1) shows bright red simple concentric zoning. The inclusion-rich zones, best visible in (e), have mottled CL appearance. The second generation of saddle dolomite (sd2) shows oscillatory zoning of mainly non- and minor red-growth bands, capped by a brightly luminescent inclusion-rich layer (yellow arrows). Sd3 shows zonation pattern similar to sd2 but with lower intensity. The final saddle dolomite cement (sd4) is non-luminescent. Small remaining pore space was filled by dull orange luminescing calcite (cal). **(g)** Fracture-filling saddle dolomite and fractured coarse crystalline, nonplanar-a dolomite matrix dolomite (md). (Location VA) **(h)** CL image of (g). The first phase of the saddle dolomite (sd1) is inclusion-rich and is characterized by bright red mottled CL (note the microfractures cross-cutting sd1). The second phase (sd2) is less turbid in transmitted light and shows simple and/or oscillatory zonation similar to sd2 in image (f). The final saddle dolomite (sd3) is similar to sd2 in transmitted light but displays bright red, homogenous CL. **(i)** Zones of saddle dolomite cement (sd) selectively replaced by calcite (cal). The dark solid inclusions along and within the calcite are likely iron hydroxides. Stained thin section. Plane-polarized light. (Location VA)

Fig. 7: Petrographic features of calcite cements. **(a)** Dolomite breccia with blocky calcite cement (CAL-2). Plane-polarized light. (Location GF-1) **(b)** CL image of (a). The blocky calcite cement displays bright orange CL. **(c)** Subhedral to euhedral, scalenohedral calcite cement in a GF-1 core sample. **(d)** Hand specimen of very fine crystalline dolomite cross-cut by whitish–transparent calcite vein. (Location VP-2) **(e)** CL photomicrograph of the sample shown in (d) displaying non-luminescent calcite with a single thin bright orange CL zone. (Location VP-2) **(f)** Hand specimen of a dolomite breccia. Clasts are made up of very fine crystalline dolomite and

the cement around the clasts is saddle dolomite. The breccia is cross-cut by a brownish calcite vein (CAL-3). (Location VP-2) **(g)** CL photomicrograph of the sample shown in (f). Dull saddle dolomite (sd) is cross-cut by a coarse crystalline, blocky calcite vein (cal). The calcite is mostly non-luminescent with bright orange/yellow oscillatory zonation likely indicating the location of nucleation. (Location VP-2) **(h)** Hand specimen of brown bladed calcite cement (CAL-3). (Location RV) **(i)** CL image of a stylolite cross-cutting a fine crystalline dolomite. The stylolite is partially filled with non-luminescent calcite. Blue and green particles are detrital silicate grains. (Location RV)

Fig. 8: Carbon and oxygen isotope plot for matrix dolomites, saddle dolomite cements, limestones and calcite cements. The colored symbols refer to the type and location of the samples, and the colored rectangles indicate the estimated composition of dolomites and calcites formed in various fluids.

Fig. 9: Plots for clumped isotope data measured on matrix dolomite samples. Legend is the same as in Fig. 8. Symbols with brown outline mark samples for which Sr isotope data is not available (see Fig. 11b–c). **(a)** Relationship between temperatures converted from Δ_{47} and calculated $\delta^{18}O$ values of the diagenetic fluids. **(b)** Relationship between temperatures converted from Δ_{47} and measured $\delta^{18}O$ of matrix dolomites.

Fig. 10: Sr isotope secular curve of the Mesozoic Era (after McArthur et al., 2012) with range of values measured on the studied samples indicated by the red bar. N = number of analyzed samples.

Fig. 11: Plots of Sr isotope vs. **(a)** $\delta^{18}O$ values of dolomite and limestone samples; **(b)** temperatures converted from Δ_{47} and **(c)** $\delta^{18}O$ values of diagenetic fluids. Legend is the same as in Fig. 8. Symbols with brown outline mark matrix dolomite samples for which clumped isotope data is not available. Otherwise, matrix dolomite samples are the same in (a), (b) and (c), and in Fig. 9.

Fig. 12: Summary of the major diagenetic processes with estimated timing, burial setting, as well as inferred diagenetic fluids and tectonic events. Dashed line indicates that the saddle dolomite cementation event likely occurred in multiple episodes with evolving fluid compositions.

Fig. 13: Schematic evolution history of the Csukma Formation from the Middle Triassic until the Early Cretaceous. Drawings are not to scale. **(a)** Stage 1: Middle Triassic. Penecontemporaneous reflux dolomitization of the Kán Dolomite Member Geothermal circulation in the middle ramp prevents invasion of brines into the Kozár Limestone Member **(b)** Stage 2: Late Early Jurassic. Increasing burial results in recrystallization of the Kán Dolomite Member in intermediate burial setting (ca. 1 to 2 km). **(c)** Stage 3: Early Cretaceous. Seawater is drawn down and circulated through rift-related faults (black lines) and causes recrystallization of the Kán Dolomite Member a second time, and dolomitization of the Kozár Limestone Member and the underlying limestones in the vicinity of the faults (indicated by grey shading) in a deep burial setting (ca. 5 km).

Tables

Table 1

Location ID	Name	Description
AT	Árpád-tető	Partially to completely dolomitized Middle Triassic limestones exposed in an abandoned quarry, and in a road-cut (Kozár Limestone Member?)
GF-1	Gálosfa-1	Kán Dolomite Member cored by the Gf-1 borehole between 910.4 m to 1195.5 m
HR	Hetvehely road-cut	Uppermost part of the Zuhánya Limestone, and lower part of the Kán Dolomite exposed in a road-cut near the town of Hetvehely
MR	Misina road-cut	Kozár Limestone exposed in a road-cut leading up to the TV tower located on Misina-tető
RV	Rák Valley	Parts of the Kán Dolomite Member exposed in the Rák Valley near the town of Gorica
VA	Váralja	Middle Triassic fine to coarse crystalline dolomites exposed in an abandoned quarry near the town of Váralja in the area of the Northern Imbricates
VP-2	Vágotpuszta-2	Irregular alternation of very fine and medium to coarse crystalline dolomites in the core section between 79 and 188 m, Kán Dolomite Member

Table 2

Sample ID	$\delta^{18}O$ (‰ V-PDB)	$\delta^{13}C$ (‰ V-PDB)	Type	$^{87}Sr/^{86}Sr$	Δ_{47} (‰)		T (°C)			$\delta^{18}O_{fluid}$ (‰ V-SMOW)
					mean	SE	mean	min.	max.	
AT NKF 1	–2.2	3.8	MC	0.70781						
AT NKF 3	–8.4	0.3	LMST	0.70798						
AT NKF 4	–8.9	2.7	MC							
AT NKF 6	–7.8	1.7	LMST							
AT UB 1	–6.6	3.4	MC							
AT UB 2	–7.8	2.5	SD							
AT UB 5a	–12.1	2.0	SD	0.70794						
AT UB 5a	–11.2	1.5	MC							
AT UB 5a	–10.9	0.6	SD							
GF-1 910.4 m	–6.2	2.4	MC							
GF-1 911.8 m	–5.3	2.6	MC							
GF-1 913.3	–5.1	2.5	VF							
GF-1 918.2 m 01	–5.6	2.2	MC							
GF-1 918.2 m 02	–6.7	2.4	MC							
GF-1 921.8 m	–5.8	2.6	MC							
GF-1 926.6 m	–8.0	2.2	MC							
GF-1 934.2 m	–4.7	2.3	VF							
GF-1 943.6 m	–3.5	2.9	VF							
GF-1 954.6 m	–8.4	2.3	VF							
GF-1 957.3 m	–6.9	2.1	MC							
GF-1 957.9 m 01	–7.4	1.8	MC							
GF-1 957.9 m 02	–7.4	1.8	MC							
GF-1 961.4 m	–4.9	1.7	VF							
GF-1 965.6 m 01	–5.0	2.1	VF							
GF-1 965.6 m 02	–7.7	1.8	MC							
GF-1 965.6 03	–7.8	1.0	MC							
GF-1 965.8 m	–3.4	1.9	VF							
GF-1 966.2 m	–3.8	1.4	VF							
GF-1 972 m	–2.4	2.3	VF							
GF-1 981.5 m	–2.8	2.9	VF							
GF-1 982 m	–3.9	2.6	VF							
GF-1 982.9 m	–2.9	1.9	VF							
GF-1 988.3 m	–2.6	1.8	VF							
GF-1 992 m	–4.5	1.9	VF							
GF-1 998 m	–4.0	1.7	VF							
GF-1 1002 m	–4.9	2.3	VF							
GF-1 1017 m	–6.7	2.6	MC							

GF-1 1032.3 m	–2.3	2.2	VF							
GF-1 1055 m	–4.1	2.1	VF	0.70819	0.576	0.005	67	64	69	2.6
GF-1 1109 m 01	–2.8	2.4	VF							
GF-1 1109 m 02	–2.7	2.6	VF							
GF-1 1147 m	–2.2	1.1	VF							
GF-1 1181.5 m	–12.4	-0.3	CAL							
GF-1 1195.5 m 01	–8.6	2.4	MC							
HR-HH 01	–8.5	2.5	MC							
HR-HH 03	–10.5	2.4	MC							
HR-HH 04	–6.3	3.0	MC							
HR-HH 08/1	–12.5	2.3	SD							
HR-HH 08/2	–12.6	2.1	MC	0.70797	0.482	0.007	127	121	132	1.3
HR-HH 18/1	–10.2	2.4	MC							
HR-HH 18/2	–10.4	2.2	MC		0.501	0.01	112	105	119	2.6
HR-HH 21 -01	–7.5	-8.2	CAL							
HR-HH 21 -02	–8.8	3.5	SD							
HR-HH 22	–4.9	2.7	VF							
HR-HH 26	–3.8	2.5	VF	0.70815	0.575	0.005	67	65	70	3.0
HR-HH 26 - H1	–4.5	2.7	VF							
HR-HH 2/1	–7.7	4.2	MC	0.70785						
HR-HH 2/2	–6.3	2.7	MC							
MR-DKA 01	–9.9	0.2	LMST							
MR-DKA 02	–7.2	2.2	LMST							
MR-DKA 03	–8.2	1.8	LMST							
MR-DKA 04	–7.4	1.6	LMST							
MR-DKA 05	–8.9	-2.2	LMST							
MR-DKA 06	–8.4	-1.3	LMST							
MR-DKA 07	–9.0	-1.5	LMST							
MR-DKA 08	–10.5	-0.9	SD							
MR-DKA 08	–8.8	-1.6	LMST							
MR-DKA 09	–9.0	-0.9	LMST							
MR-DKA 10	–9.2	-2.7	LMST							
MR-DKA 11	–8.4	-1.2	LMST							
MR-DKA 12	–8.8	-1.1	LMST							
MR-DKA 13	–9.6	-1.7	LMST							
MR-DKA 14	–8.9	0.1	LMST							
MR-DKA 15	–9.0	-3.3	LMST	0.70802						
RV-GO-1/1	–7.8	-8.5	CAL							
RV-GO-3/1	–3.2	1.9	VF							
RV 2	–7.2	3.2	MC							
VA 03 -01	–5.5	2.7	MC							
VA 03 -02	–10.3	0.8	SD							
VA 06	–6.5	2.4	MC							

VA 07	–10.1	1.5	MC		0.478	0.007	130	124	136	4.3
VA 09	–4.9	1.4	VF							
VA 10	–20.5	-0.9	CAL							
VA 2T/1	–13.0	0.3	SD							
VA 2T/2	–7.2	2.0	MC							
VA 3T/1	–7.5	2.4	MC	0.70780						
VA 3T/2	–15.4	1.1	SD	0.70823						
VP-2 79.3 m U1	–7.7	2.2	MC							
VP-2 79.3 m U2	–6.2	2.5	SD							
VP-2 79.3 m L	–5.3	2.3	MC							
VP-2 83.2 m	–10.3	0.1	MC	0.70790	0.508	0.012	107	99	116	1.7
VP-2 97.2 m	–9.2	1.1	MC							
VP-2 98.7 m	–6.5	0.9	MC							
VP-2 99.6 m 01	–3.2	0.4	VF							
VP-2 99.6 m 02	–10.0	1.2	SD							
VP-2 119 m 01	–6.2	-4.8	CAL							
VP-2 119 m 02	–9.0	2.6	SD							
VP-2 125.4 m	–9.4	0.9	SD							
VP-2 154.2 m	–2.0	2.4	VF	0.70813	0.611	0.006	50	48	53	2.0
VP-2 160.3 m 01	–4.2	2.5	VF							
VP-2 160.3 m 02	–7.5	3.7	SD							

Figures

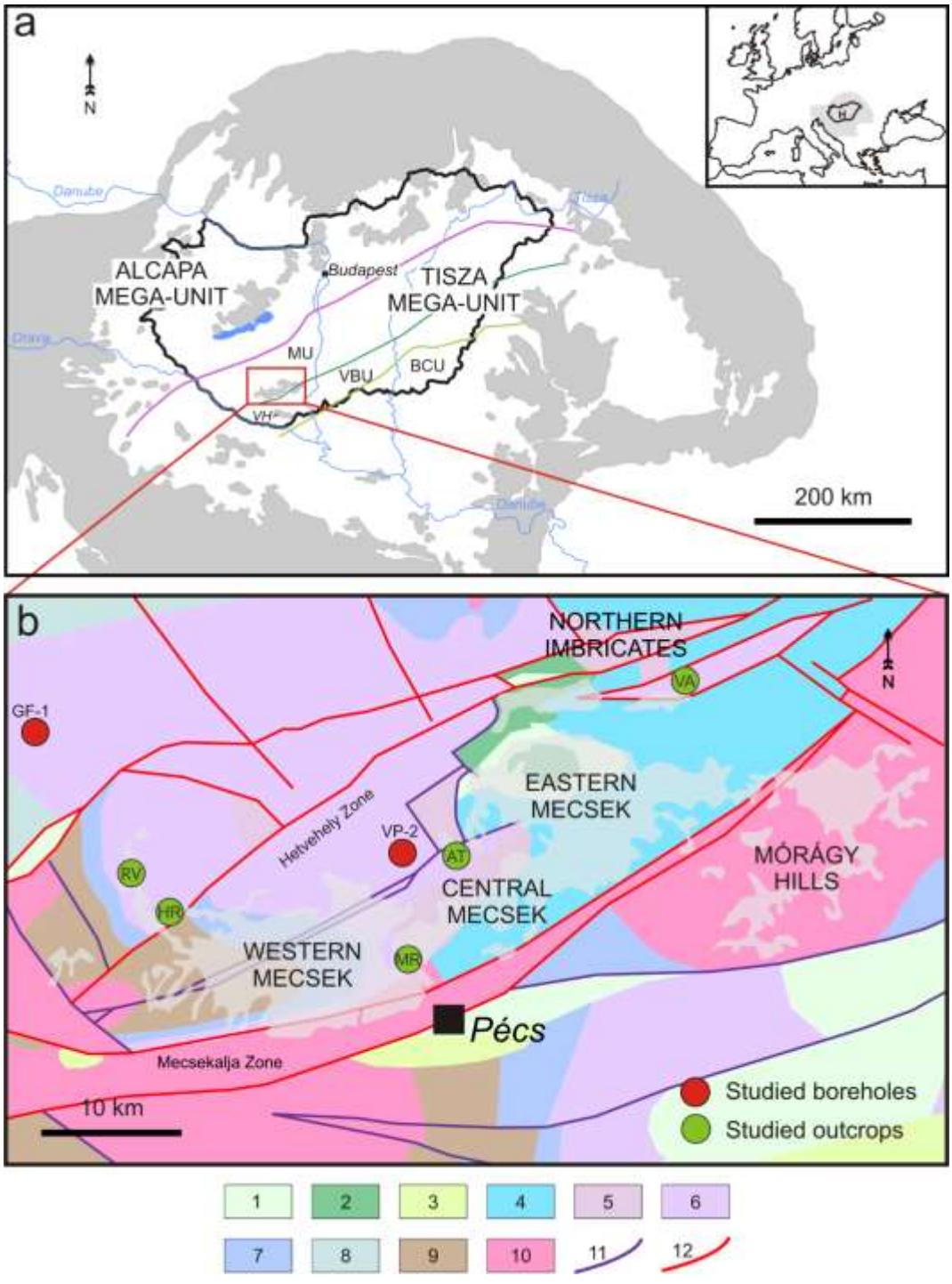

Fig. 1.

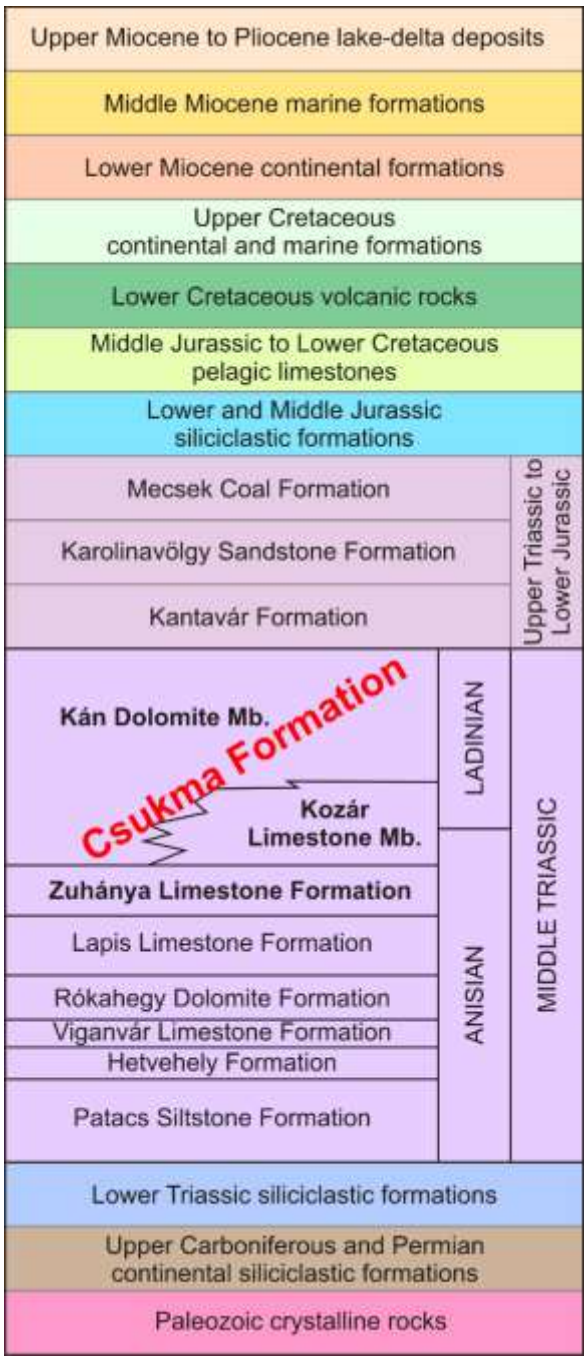
Upper Miocene to Pliocene lake-delta deposits
Middle Miocene marine formations
Lower Miocene continental formations
Upper Cretaceous
continental and marine formations
Lower Cretaceous volcanic rocks
Middle Jurassic to Lower Cretaceous
pelagic limestones
Lower and Middle Jurassic
siliciclastic formations
Mecsek Coal Formation
Karolinavölgy Sandstone Formation
Kantavár Formation
Upper Triassic to Lower Jurassic
Kán Dolomite Mb.
Csukma Formation
Kozár
Limestone Mb.
LADINIAN
Zuhánya Limestone Formation
Lapis Limestone Formation
Rókahegy Dolomite Formation
Viganvár Limestone Formation
Hetvehely Formation
Patacs Siltstone Formation
ANISIAN
MIDDLE TRIASSIC
Lower Triassic siliciclastic formations
Upper Carboniferous and Permian
continental siliciclastic formations
Paleozoic crystalline rocks

Fig. 2

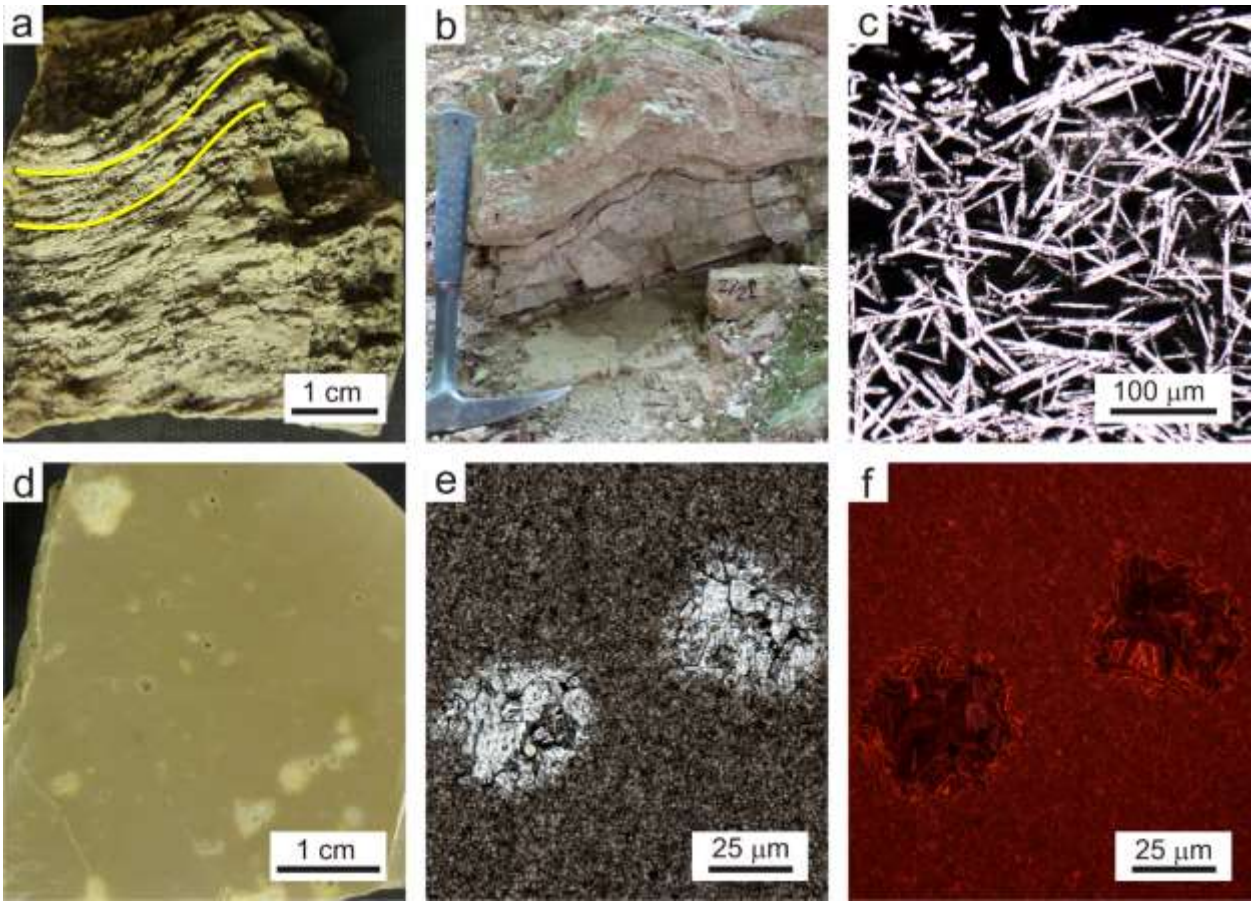

Fig. 3

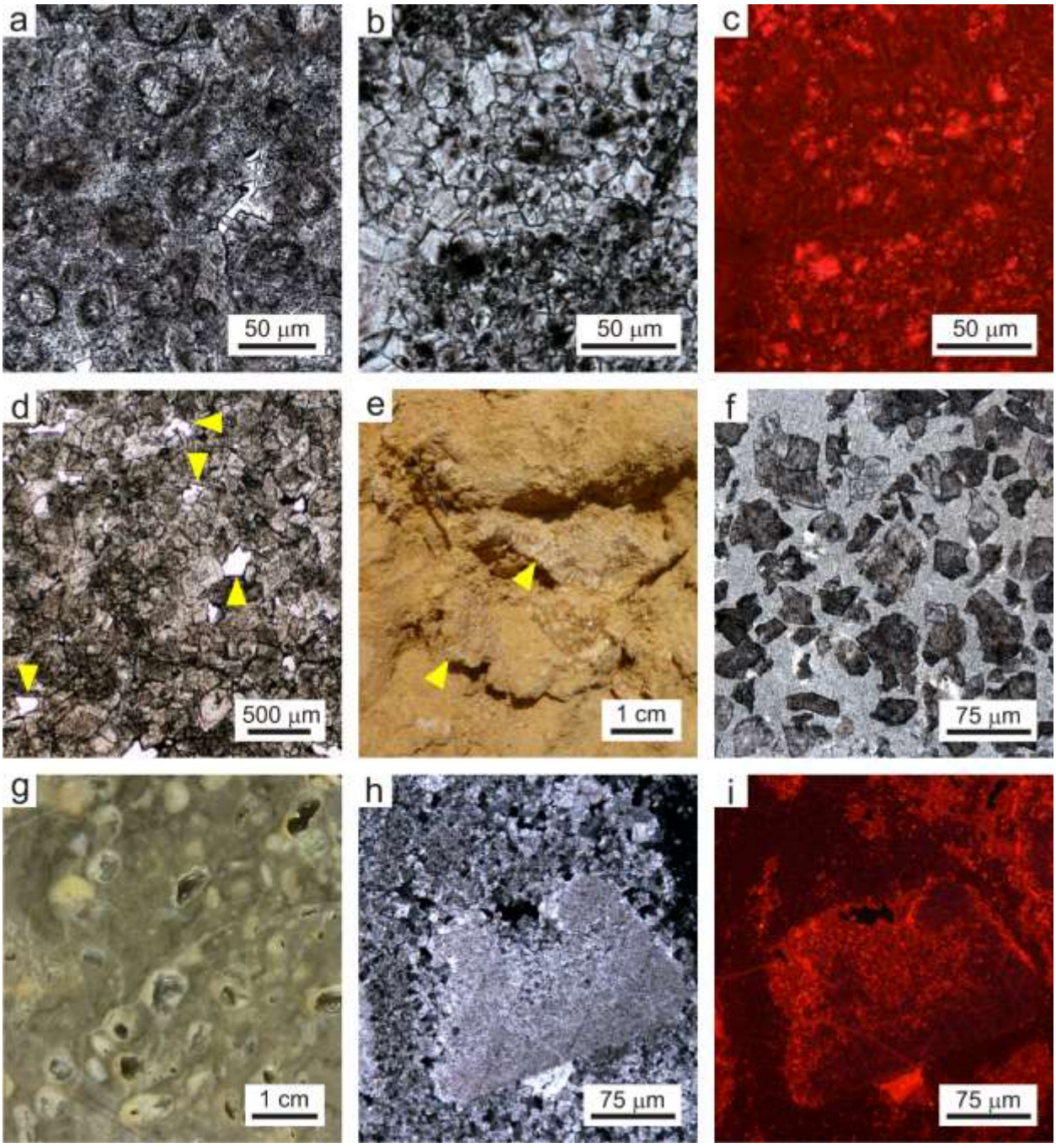

Fig. 4

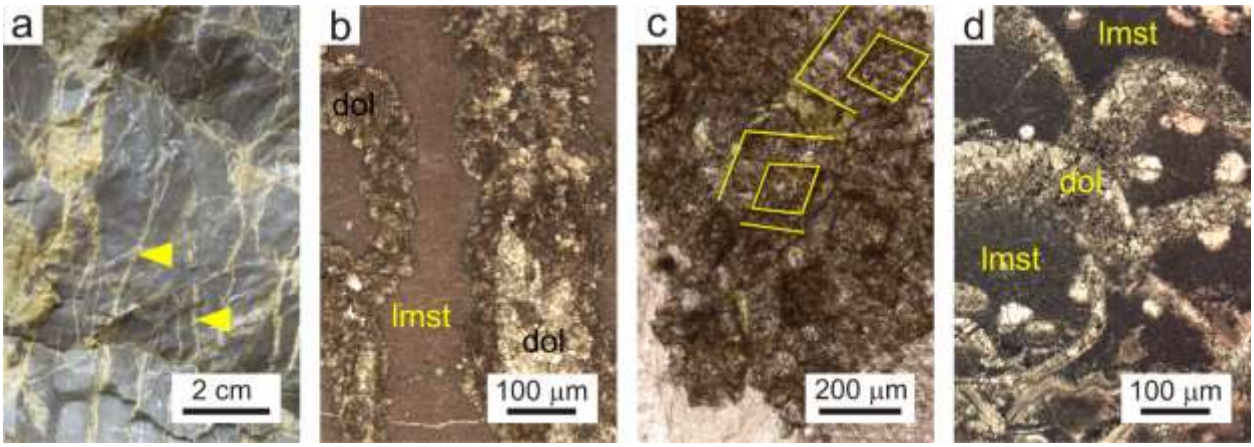

Fig. 5

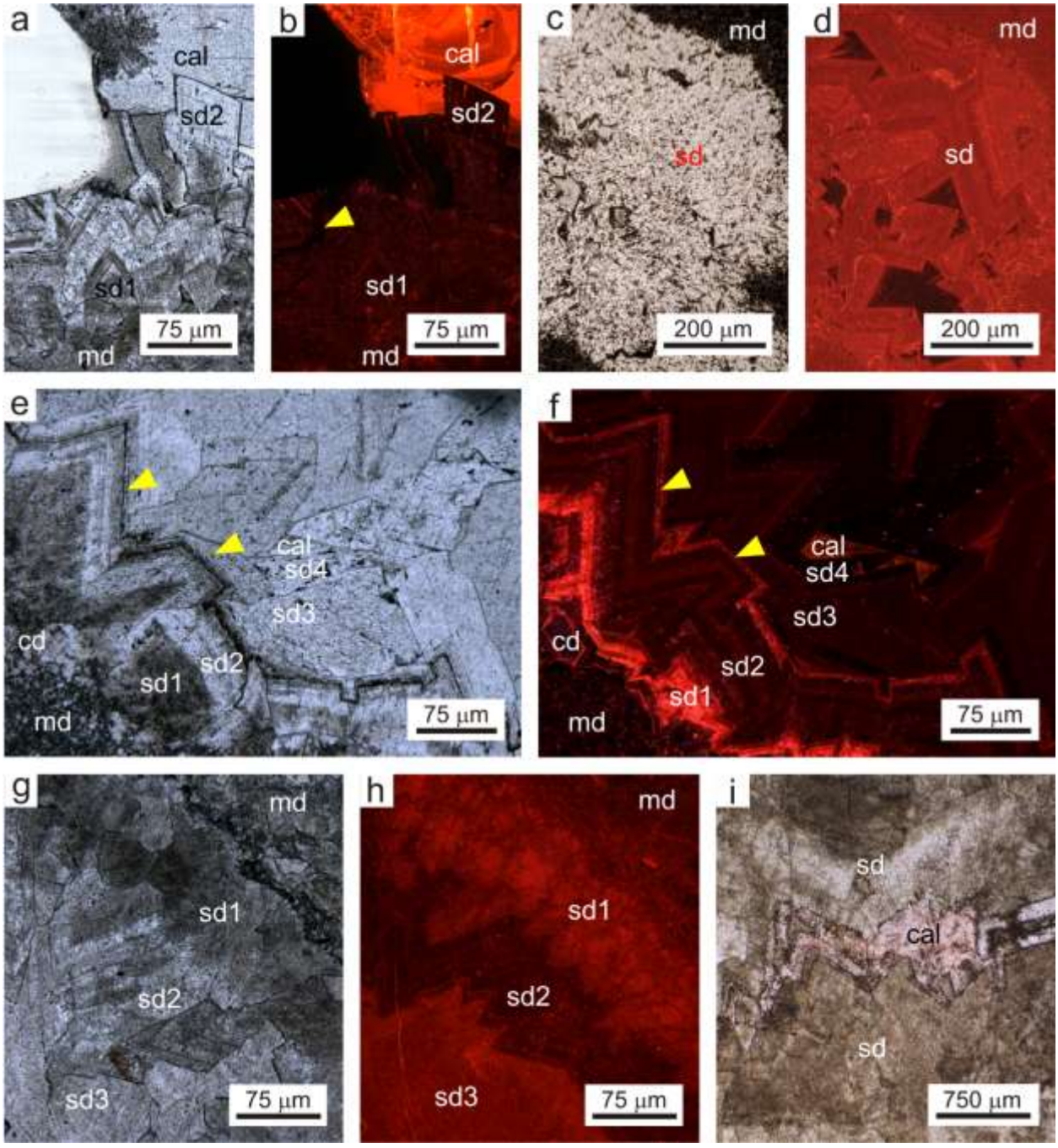
a
cal
sd2
sd1
md
75 μm
b
cal
sd2
sd1
md
75 μm
c
md
sd
200 μm
d
md
sd
200 μm
e
cal
sd4
sd3
cd
sd2
sd1
md
75 μm
f
cal
sd4
sd3
cd
sd2
sd1
md
75 μm
g
md
sd1
sd2
sd3
75 μm
h
md
sd1
sd2
sd3
75 μm
i
sd
cal
sd
750 μm

Fig. 6

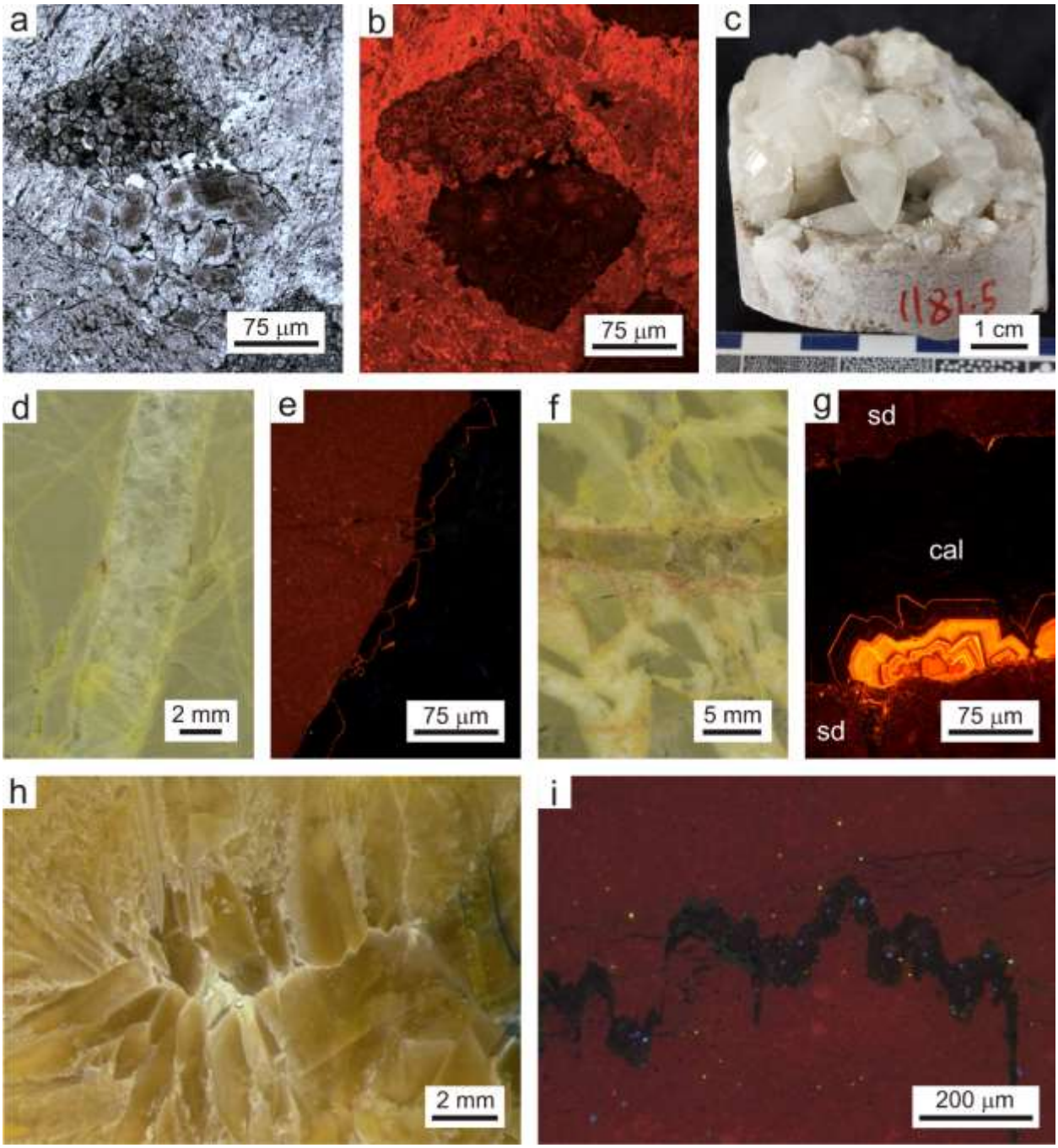
a
75 μm
b
75 μm
c
1181.5
1 cm
d
2 mm
e
75 μm
f
5 mm
g
sd
cal
sd
75 μm
h
2 mm
i
200 μm

Fig. 7

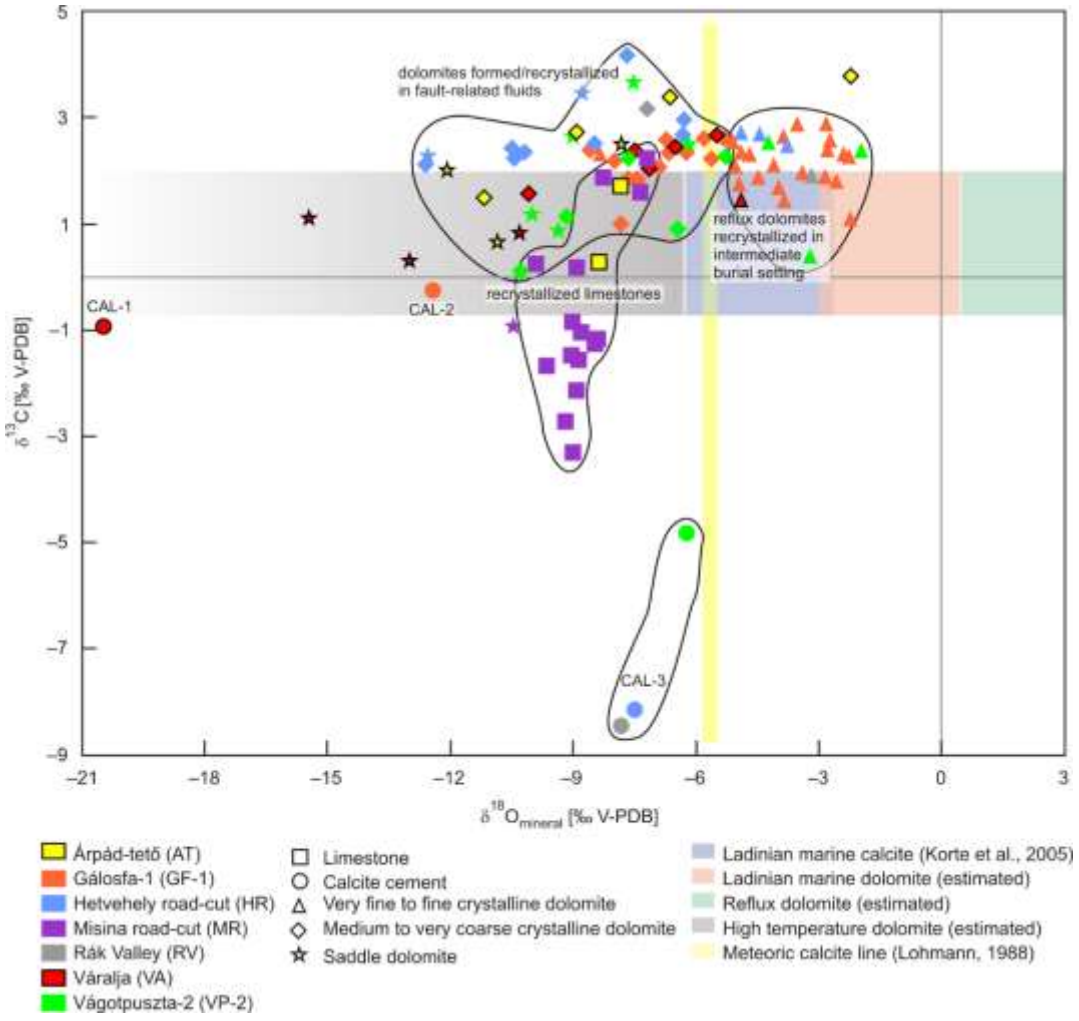
dolomites formed/recrystallized in fault-related fluids
reflux dolomites recrystallized in intermediate burial setting
recrystallized limestones
CAL-1
CAL-2
CAL-3
δ13C [‰ V-PDB]
δ18Omineral [‰ V-PDB]
Árpád-tető (AT)
Gálosfa-1 (GF-1)
Hetvehely road-cut (HR)
Misina road-cut (MR)
Rák Valley (RV)
Váralja (VA)
Vágotpuszta-2 (VP-2)
Limestone
Calcite cement
Very fine to fine crystalline dolomite
Medium to very coarse crystalline dolomite
Saddle dolomite
Ladinian marine calcite (Korte et al., 2005)
Ladinian marine dolomite (estimated)
Reflux dolomite (estimated)
High temperature dolomite (estimated)
Meteoric calcite line (Lohmann, 1988)

Fig. 8

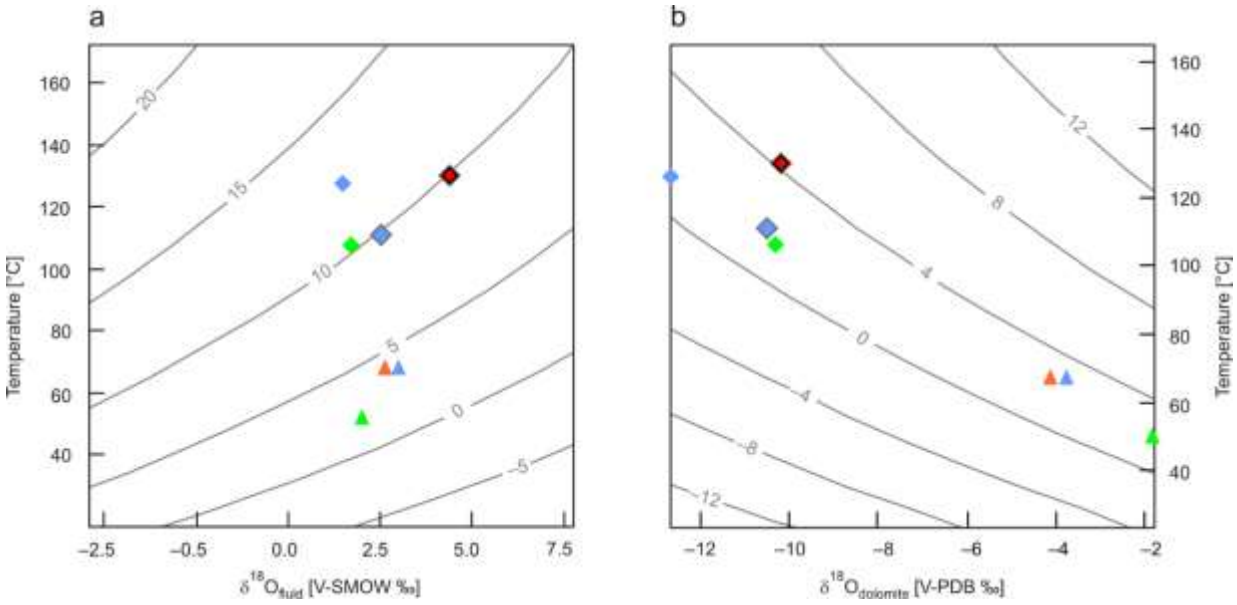
a
b
Temperature [°C]
160
140
120
100
80
60
40
20
15
10
5
0
−5
−2.5
−0.5
0.0
2.5
5.0
7.5
δ18Ofluid [V-SMOW ‰]
12
8
4
0
−4
−8
−12
−12
−10
−8
−6
−4
−2
δ18Odolomite [V-PDB ‰]

Fig. 9

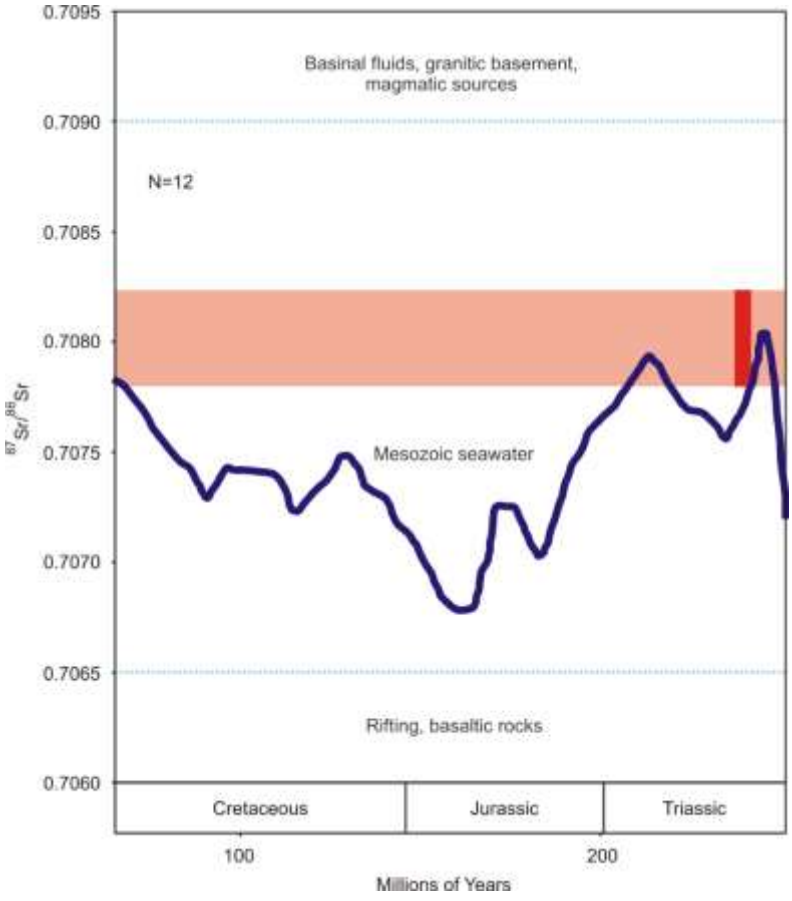
0.7095
0.7090
0.7085
0.7080
0.7075
0.7070
0.7065
0.7060
$^{87}Sr/^{86}Sr$
Basinal fluids, granitic basement,
magmatic sources
N=12
Mesozoic seawater
Rifting, basaltic rocks
Cretaceous
Jurassic
Triassic
100
200
Millions of Years

Fig. 10

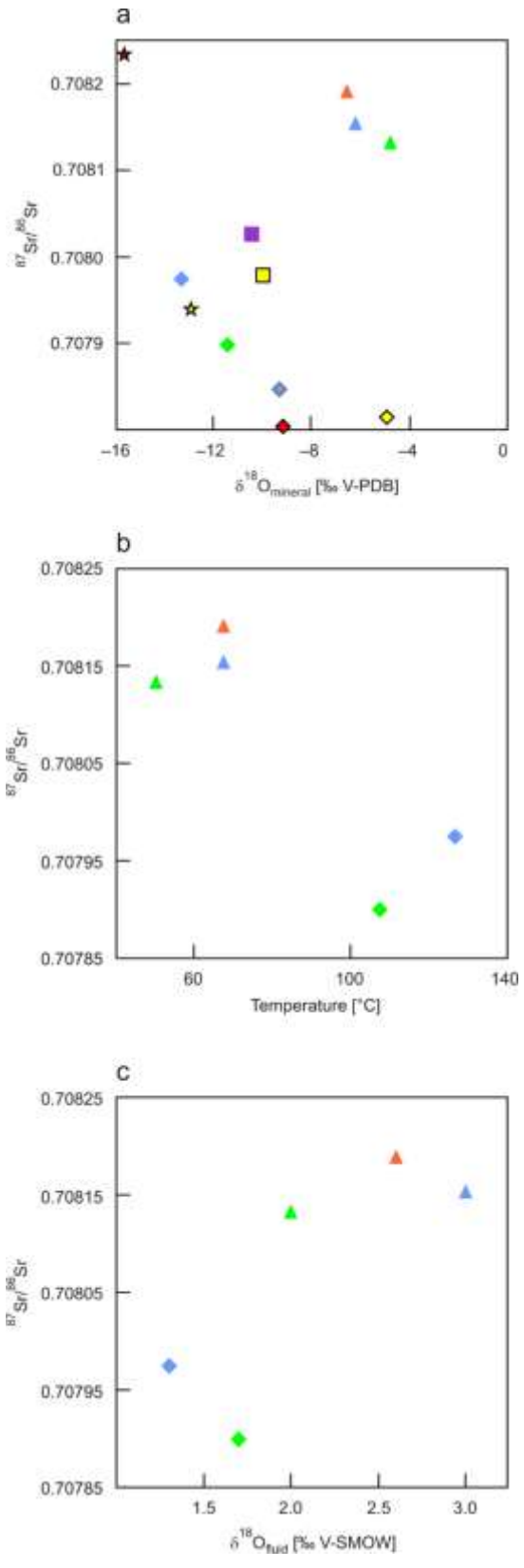
a
0.7082
0.7081
0.7080
0.7079
$^{87}Sr/^{86}Sr$
−16
−12
−8
−4
0
$\delta^{18}O_{mineral}$ [‰ V-PDB]
b
0.70825
0.70815
0.70805
0.70795
0.70785
$^{87}Sr/^{86}Sr$
60
100
140
Temperature [°C]
c
0.70825
0.70815
0.70805
0.70795
0.70785
$^{87}Sr/^{86}Sr$
1.5
2.0
2.5
3.0
$\delta^{18}O_{fluid}$ [‰ V-SMOW]

Fig. 11

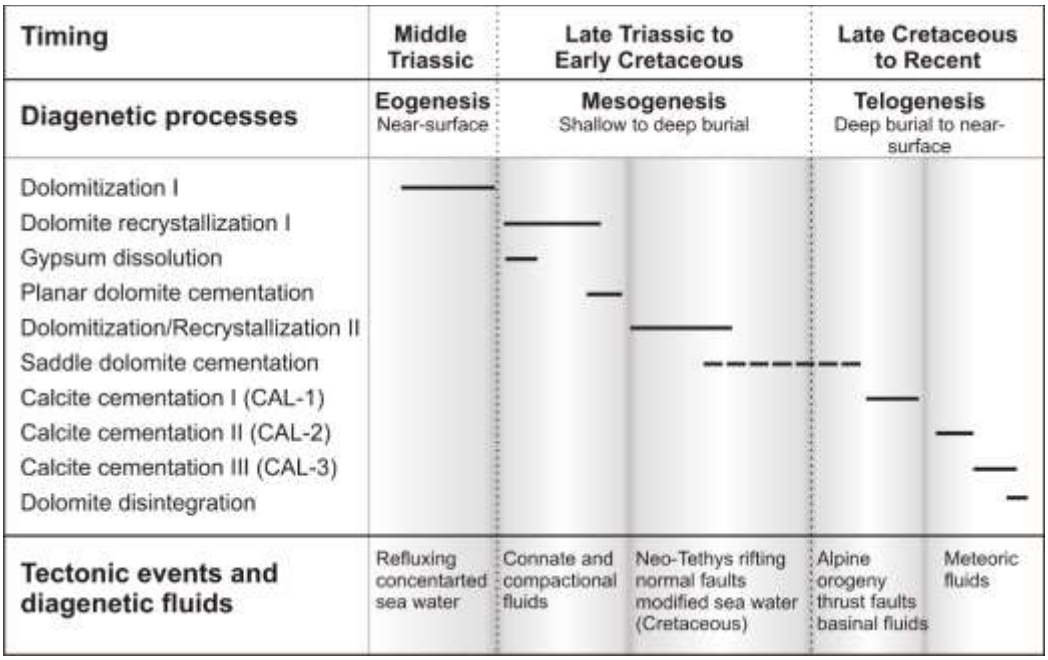
Timing
Middle Triassic
Late Triassic to Early Cretaceous
Late Cretaceous to Recent
Diagenetic processes
Eogenesis
Near-surface
Mesogenesis
Shallow to deep burial
Telogenesis
Deep burial to near-surface
Dolomitization I
Dolomite recrystallization I
Gypsum dissolution
Planar dolomite cementation
Dolomitization/Recrystallization II
Saddle dolomite cementation
Calcite cementation I (CAL-1)
Calcite cementation II (CAL-2)
Calcite cementation III (CAL-3)
Dolomite disintegration
Tectonic events and diagenetic fluids
Refluxing concentarted sea water
Connate and compactional fluids
Neo-Tethys rifting normal faults modified sea water (Cretaceous)
Alpine orogeny thrust faults basinal fluids
Meteoric fluids

Fig. 12

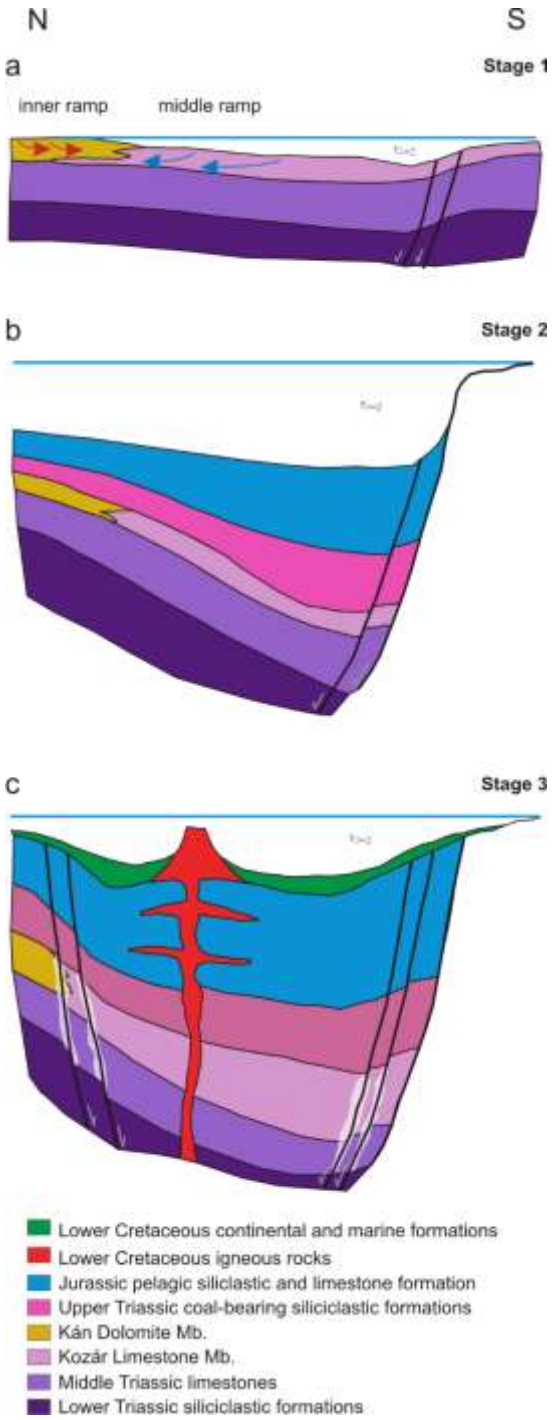
N
S
a
Stage 1
inner ramp
middle ramp
b
Stage 2
c
Stage 3
Lower Cretaceous continental and marine formations
Lower Cretaceous igneous rocks
Jurassic pelagic siliclastic and limestone formation
Upper Triassic coal-bearing siliciclastic formations
Kán Dolomite Mb.
Kozár Limestone Mb.
Middle Triassic limestones
Lower Triassic siliciclastic formations

Fig. 13